Exploring the ocean for hydrothermal venting: New techniques, new discoveries, new insights

Edward T. Baker[a]

[a] Joint Institution for the Study of the Atmosphere and Ocean, University of Washington, and NOAA/PMEL, Seattle WA 98115 USA (E-mail: edward.baker@noaa.gov)

Abstract

Enumerating active hydrothermal fields on the seafloor has been a challenge since their discovery almost 40 years ago. High-temperature hydrothermal fields are readily discoverable, primarily by detecting mineral-laden plumes, but low-temperature, particle-poor vent fields resist discovery. Decades of exploration for vent fields have covered, though often cursorily, about one-third of the global lengths of both oceanic spreading ridges (OSRs) and volcanic arcs, identifying some 630 active vent fields. About 80% of these fields are on OSRs, and the spatial frequency of those fields is currently estimated as ~0.5–5/100 km, generally increasing with spreading rate. Over the last decade, however, a few detailed surveys have added sensors capable of detecting ephemeral chemical tracers (oxidation-reduction potential) in addition to standard sensors that detect quasi-conservative optical tracers (such as light backscattering). This approach has revealed a new view of the distribution of venting fields along fast-spreading (>55 mm/yr) OSRs. Studies of four such ridge sections totaling 1470 km length suggest that the present inventory of vent fields may underestimate the true global population of vent fields on fast-spreading OSRs by a factor of 3–6. This increase implies that ridge axes are unexpectedly "leaky" reservoirs, from which hydrothermal fluids escape at far more sites than presently assumed; that the supply of dissolved hydrothermal iron, which may be fertilizing the primary production of the Southern Ocean, is higher than now calculated; and that present estimates of recoverable sulfide tonnage from ridge axes may be too low. Along slow-spreading ridges, which account for 60% of the global OSR length and 86% of known sulfide tonnage, expansive axial valleys present special exploration challenges that will not be easily overcome.

Keywords: **Hydrothermal venting; diffuse flow; ocean ridges; faunal distribution; geochemical budgets; crustal circulation**

1. Introduction

Evidence that magmatic heat can be readily transferred to the deep ocean goes back to the 1960s. Samples of hot brine were collected at the bottom of the Red Sea (Miller et al., 1966), a continental rift, and Knauss (1962) suggested that abnormally warm water between 3000 and 3500 m over the East Pacific Rise (EPR) near 20°S was related to a recently mapped zone of high seafloor heat flow in the same area. In the 1970s, discoveries of enhanced concentrations of hydrothermal tracers such as ^{3}He above the EPR (Craig et al., 1975) and dissolved Mn above the Galápagos Spreading Center (GSC) (Klinkhammer et al., 1977) dramatically verified these observations. The culmination of these observations, and the dawn of the hydrothermal age, was the discovery of hydrothermal fluids discharging as low-temperature diffuse flow on the GSC in 1977 (Corliss et al., 1979) and as high-temperature black smokers on the EPR at 21°N in 1979 (Spiess et al., 1980).

Exploration for vent fields began initially by means of seafloor imaging using submersibles and towed cameras (e.g., Ballard et al., 1984; McConachy et al., 1986). Concurrently, water column sampling revealed that hydrothermal venting created plumes above vent fields as hot, buoyant fluids rose, entrained ambient seawater, and dispersed laterally along density isolines after reaching buoyancy equilibrium (Lupton et al., 1980). Oceanographers soon found that plumes could be detected not only by collecting and analyzing water samples, but also by real-time measurements of temperature and optical (light transmission or backscattering) signatures. By slowly towing such sensors behind a ship along a ridge crest, these tracers could map a two-dimensional transect of plumes along tens to hundreds of kilometers (Baker et al., 1985). This technique swiftly located seafloor vent fields to within several kilometers, making follow-up searches by submersibles and remotely operated vehicles (ROV) far more efficient.

In the first decade or so of hydrothermal studies, geologists debated whether the primary control on the distribution of vent fields was heat supply (primarily from cooling magma) or tectonic setting (regulating the access of seawater to crustal heat). Extrapolating from hydrothermal plumes mapped along the Juan de Fuca Ridge in the northeast Pacific, Baker and

Hammond (1992) hypothesized that the spatial frequency of such plumes, and thus of vent fields themselves, increased linearly with spreading rate (a proxy for the magma budget) for all ridges. Accumulating plume data from fast-spreading (>55 mm/yr) ridges strengthened this hypothesis (Baker et al., 1996). However, surveys along the Mid-Atlantic Ridge (MAR) suggested that the relationship was more complicated along slow-spreading ridges. German and Parson (1996), for example, found that plume frequency was elevated in settings where magma supply was limited but tectonic activity had apparently increased bulk crustal permeability and thus the accessibility to other sources of crustal heat. Understanding the complexity of hydrothermal venting along slow-spreading ridges remains a major research theme (e.g., Rona et al., 2010; German et al., 2016).

Since the late 1990s, several developments have contributed to maintaining the pace of vent field discovery. First, the systematic exploration of the Kermadec arc (de Ronde et al., 2001) found abundant active hydrothermalism, thus energizing interest in arcs (Baker et al., 2008a) and back-arc spreading ridges (BASCs) (Martinez et al., 2006; German et al., 2006) of the western Pacific. Second, opportunities to detect hydrothermal plumes were expanded by the introduction of a simple autonomous optical and (later) chemical sensor that could be added to any wire used in shipboard operations (e.g., rock dredges, rock cores, deep-towed sonar systems) (e.g., Edmonds et al., 2003). The widespread availability of Miniature Autonomous Plume Recorders (MAPRs) developed by the NOAA Pacific Marine Environmental Laboratory (PMEL) has, since 1996, led to the discovery of almost 200 vent fields (Hammond et al., 2015). And, more recently, commercial (e.g., http://www.nautilusminerals.com) and state-sponsored (Kim et al., 2009; Tao et al., 2012) interest in locating minable seafloor massive sulfides (SMS) has driven exploration for vent fields along western Pacific arcs and BASCs, and on ultraslow-spreading ridges in the Indian Ocean.

In this paper I first review the history of vent field exploration, describing the known distribution of active vent fields in terms of tectonic settings, water depth, and jurisdictional boundaries. I then explain how the application of “best practices” in exploration and the use of new sensor technology reveal that our current inventory of the global vent field population may be greatly underestimated. Finally, I discuss how these new results can affect our understanding of several important processes operating at the Earth-ocean boundary.

2. Results from past exploration

The InterRidge Database (http://vents-data.interridge.org) is the authoritative repository of active vent field locations, but is subject to biases that inherently reduce its comprehensiveness. The database defines a vent field as "a cluster or assemblage of venting sites in relatively close proximity (i.e., on the order of 0.1–1 km)," and the same definition is used here. Off-axis vent fields are excluded. It relies on information from published papers, and so favors named fields listed in these papers rather than a rigorous analysis of the underlying data. Because the most common plume detection tools are optical (light transmission or scattering) sensors, exploration has been strongly biased toward the discovery of high-temperature, black smoker venting (Fig. 1a-c). Isolated, low-temperature fields are likely overlooked (Larson et al., 2015) (Fig. 1d-f). And the preponderance of hydrothermal survey efforts that utilize discrete vertical profiles, rather than spatially continuous observations, inevitably results in undercounting fields.

As of 2016, active submarine vent fields in the InterRidge Database numbered more than 630 and have been found along the boundaries of 46 out of 52 recognized tectonic plates (Beaulieu et al., 2013, 2015) (Fig. 2). Forty-five percent of the fields have been confirmed visually. The remainder is known only by inference from plume anomalies in the water column. About 80% of all fields have been detected first by water column surveys rather than by seafloor discovery. The rate of vent field discovery has been remarkably steady at 20/yr since the early 1980s, with new mid-ocean ridge (MOR) vent fields being logged about twice as fast as those on arcs and BASCs (Fig. 3). Between ~2000 and 2010, an increase in the discovery rate of vent fields on arcs and BASCs resulted in a decline in the discovery of MOR sites. The near-constant overall discovery rate, including the compensating changes in MOR and arc/BASC discoveries in the early 2000s, suggests that the global resources applied to hydrothermal exploration have changed little in many decades.

2.1. Ocean spreading ridges

Ocean Spreading Ridges (OSRs, the sum of MORs and BASCs) total 71,000 km and account for ~75% (484) of all known vent fields. Three-quarters of those occur on MORs.

Because total ridge length increases with declining spreading rate, the total number of discovered vent fields on OSRs also declines roughly with increasing spreading rate (Fig. 4a). Conversely, vent field spatial frequency, F_s (fields/100 km of strike length), increases with spreading rate (Fig. 4b), corresponding to an increase in the magma budget and thus available heat sources. The mean F_s from the global dataset is 1.1±0.91. However, much of the variability in this global view of F_s is a function of exploration history.

To obtain a more accurate estimate of how F_s varies with spreading rate, and thus to better predict the total inventory of vent fields, we examine only well-surveyed ridge sections. Beaulieu et al. (2015), using the InterRidge Database, identified 27 lengthy (>240 km) sections spanning the entire range of spreading rates (Table 1). Scatter among these 27 sections is expected due to differences in survey effort (e.g., survey length, continuous or discrete sampling) and uncertainty in discriminating individual vent fields from water column data.

A linear regression of F_s against full spreading rate gives:

$$F_s = 0.81 + 0.024u_s,\ r = 0.53,$$

where u_s is weighted average full spreading rate (mm/yr) for each section (Fig. 5). The most distant outlier and highest F_s value is the Eastern Lau Spreading Center (ELSC), a BASC section adjacent to the Kermadec volcanic arc, where spreading rates increase from 39 to 96 mm/yr from south to north (Zellmer and Taylor, 2001). The ELSC has been a sustained focus of hydrothermal exploration, undergoing multiple repeat plume surveys in both 2004 and 2008, thus greatly increasing the likelihood of vent field discovery. Also, the closeness of the southern end of the ELSC to the Kermadec arc (~40 km) may increase the magmatic heat available for venting above that normally available to a ridge spreading at ~40 mm/yr (Martinez et al., 2006).

We obtain a clearer view of the relationship between spreading rate and F_s by binning the data according to standard spreading-rate intervals (Fig. 5). At any given spreading rate, hydrothermal activity varies spatially because different ridge sections can express different stages of magmatic or amagmatic evolution (e.g., Macdonald and Fox, 1988). The larger the sample size (i.e., ridge length surveyed) at a given spreading rate, the more representative the F_s value. Thus, for the binned values:

$$F_s = 0.76 + 0.022u_s,\ r = 0.96.$$

This fit has slope and intercepts little different than the unbinned regression but greatly increases the correlation coefficient. This regression is slightly different than that of Beaulieu et al. (2015), where only 21 of the 27 ridge segments were used.

Based on the binned data, a more representative global mean F_s value (at the global mean spreading rate of 50 mm/yr) is 1.9 fields/100 km. Mean spacing of known vent fields thus ranges from ~25 km at superfast spreading (F_s = 4.1 at 150 mm/yr) to ~100 km at ultraslow spreading (F_s = 1.0 at 10 mm/yr). These separation estimates are closer than those calculated using an entirely different method by Hannington et al. (2014) (174 km for "slow" ridges and 54 km for "fast") because their calculation included only those fields with SMS deposits >100 m^2. The geological implications of an F_s value of ~1 even at zero spreading rate (and presumably zero magmatic budget) remain unclear. This result could simply be a product of undersampling, given that the 95% confidence interval of the slope has an intercept value that includes F_s = 0 (Fig. 5).

It is also possible that a linear fit to the existing sample set poorly represents the true global population. Because the fastest spreading ridges are undersampled (with surveys in only two areas), the true F_s value for such ridges may be higher and thus supportive of a linear fit where F_s = 0 at zero spreading rate. Or, geological processes may dictate that the rate of vent field formation slows with increasing spreading rate, and so a nonlinear relationship is appropriate. Evaluation of such alternatives awaits further exploration.

Alternatively, we can frame a geologically based hypothesis stating that F_s on slow and ultraslow ridges exceeds the global trend because magmatic heat is supplemented by heat from mantle rocks and serpentinization (Baker and German, 2004; German et al., 2016) (see the alternative fit in Fig. 5). Even in a magma desert, these ridges have access to significant crustal heat (Cannat et al., 2004). At a full spreading rate of 25 mm/yr, for example, the magmatic heat available for hydrothermal systems should be ~18–25 MW/km of ridge crest. For fully amagmatic spreading at the same rate, heat from cooling peridotites and serpentinization (only ~3% of the total) supplies ~16 MW/km. Even at ultraslow rates (~10 mm/yr), ~9 MW/km is available from amagmatic heat sources. A mix of magmatic segments linked by non-transform overlaps where mantle rocks are exposed could mine heat from both processes, thus leading to an abnormally high F_s value such as at 36°–38°N on the MAR (Table 1). This ridge section includes

seven magmatic segments linked by non-transform overlaps where exposed peridotites and gabbros are common (German and Parson, 1996; Gràcia et al., 2000). Nine fields have been reported on the magmatic segments, and four more in tectonic settings near the overlaps.

Assuming that the binned regression is valid, it can be used to estimate the total inventory of seafloor vent fields (Baker and German, 2004; Beaulieu et al., 2015). Applying that relation to the global distribution of ridge spreading rates binned at 10 mm/yr intervals yields a total population of 1305 (with 95% confidence limits 713–1853) (Fig. 6).

2.2. Volcanic arcs

Submarine volcanic arcs extend for fully a third of the length of OSRs, but systematic investigation of their hydrothermal venting only began in 1999 along the Kermadec arc (de Ronde et al., 2001). The 22,000 km of arcs with a submarine component are divided between 7000 km of intraoceanic arcs and 15,000 km of island arcs (de Ronde et al., 2003). The western Pacific hosts 93% (by length) of these arcs. Intraoceanic arcs have ocean crust on either side, are primarily submarine, and host an estimated 203 submarine volcanoes, of which ~43% are known to be hydrothermally active (de Ronde et al., 2003; Baker et al., 2008a). Island arcs are underlain by continental crust, are primarily subaerial, and 42% of their 57 known submarine volcanoes are hydrothermally active. On a third (by length) of island arcs, no reliable estimate of the number of submarine volcanoes yet exists (Fig. 7).

For well-explored intraoceanic arcs, such as the Mariana and Kermadec-Tonga, F_s = 1.8/100 km, comparable to OSRs. By contrast, for the explored island arcs—Aeolian, Solomon, and Tabar-Lihir-Tanga-Feni—F_s = 0.9/100 km. Assuming that these values reliably represent each volcanic arc type, we can roughly evaluate the hydrothermal impact of arcs compared to OSRs. On a distance-normalized basis, the percentage of vent fields found on arcs ($F_{s,arc}$) is:

$$F_{s,arc} = (7000 \text{ km}*(1.8/100 \text{ km}) + 15000 \text{ km}*(0.9/100 \text{ km}))/(71000 \text{ km}*(2/100 \text{ km}))$$
$$= 18\%$$

This result is less than the present percentage of known arc vent fields in the InterRidge Database (27%), probably reflecting the fact that a higher percentage of arc length (27%) than OSR length

(13%) has been well explored (Fig. 4a). Roughly then, arcs might contribute about one-fifth of the chemical discharge estimated from OSRs, provided we assume equivalent mean fluxes for individual fields on arcs and OSRs, an equivalence that remains speculative. Further, this estimate requires that F_s on the few arcs already studied is comparable to that of unexplored intraoceanic and island arcs.

Even with these qualifications, arcs are likely to be an important contributor to the global hydrothermal budget. In fact, chemically and environmentally, the impact may be even more significant than the 18% estimated here. Many important chemical species are often more highly concentrated in arc hydrothermal fluids than in OSR fluids, such as the magmatic gases CO_2-SO_2-H_2S and elemental S and Fe (de Ronde et al., 2001; Massoth et al., 2007; Resing et al., 2009). Various S and Fe species are critical nutrients for microbial life at hydrothermal ecosystems (e.g., Kelley et al., 2002). Hydrothermal flux from arcs also differs from OSR injections in that it dominates the upper 1300 m of the ocean (Fig. 8). Although no direct measurements of Fe fertilization have yet been conducted above hydrothermally active arc volcanoes, Fe introduced into shallow waters not only by volcanic eruptions (Achterberg et al., 2013) but also by shallow venting and Fe-rich metalliferous sediments (Coale et al., 1996) have been linked to increased phytoplankton production.

2.3. Global depth and jurisdictional patterns

The depth distribution of known vent fields is bimodal, dominated at depths below ~1300 m by fields on spreading ridges and at shallower depths by fields on arcs (Fig. 8). High-temperature, black smoker vents are now known to range from 345 m (East Diamante on the Mariana arc) (Embley et al., 2007) to 4960 m (Piccard/Beebe on the mid-Cayman Trough) (Connelly et al., 2012). Because the two-phase (boiling) curve for hydrothermal fluids is a function of pressure (Bischoff and Rosenbauer, 1984), depth exerts a powerful control on vent temperature. Thus, median values of the 170 reported maximum fluid temperatures in the InterRidge Database are 133°C for arc vents and 269°C for OSR vents. Nevertheless, we can surmise that a significant majority of inferred fields host high-temperature venting because most have been located by detection of an optical plume, which generally requires temperatures in excess of ~100°C (and predominantly >300°C) to produce the dissolved metals that precipitate

into particles. This majority may decline, however, as new sensor technology makes detection of low-temperature, particle-poor plumes more reliable (see Section *3.2*).

The most significant trend in the jurisdictional pattern of vent fields is the rise of hydrothermal exploration and discovery in national Exclusive Economic Zones (EEZs) since the turn of the century (Beaulieu et al., 2013). Prior to 2000, ~50% of all known vent fields were in the high seas. As of 2015, that percentage had fallen to 38%, largely due to operations in the volcanic arcs and BASCs of the western Pacific. A quarter of all vent fields discovered since 2000 occurred in the Tongan EEZ, with EEZs of the USA (Northern Mariana Islands and Guam) and New Zealand each contributing a further 5% (Fig. 9).

Commercial and National mining interests have played a key role in exploration of the western Pacific since 2000. Nautilus Minerals, Inc., has some 500,000 km^2 of granted and applied-for mining tenements (see nautilusminerals.com). The first commercial mining lease for deep-sea sulfide deposits was granted to Nautilus in 2011 by Papua New Guinea for the Solwara 1 field in the Manus Basin. National mining interests have focused on high seas regions (termed "The Area" by the International Seabed Authority, or ISA). After regulations on prospecting and exploration for polymetallic sulfides in The Area were adopted by the ISA in 2010, the first two sets of blocks (each covering 10,000 km^2) were granted in 2011 to China at the Southwest Indian Ridge and the Russian Federation at the northern MAR. Additional applications have been approved for the Republic of Korea, the Federal Republic of Germany, and the Institut Francais de Recherche pour l'Exploitation de la Mer. A minimum estimate for the number of known vent fields in areas controlled by these commercial and national interests is ~100. The political visibility of seafloor mining is emphasized by the 2015 G-7 Leaders' Declaration (see whitehouse.gov/the-press-office/2015/06/08/g-7-leaders-declaration), which specifically stated the need for regulatory certainty, investment predictability, and the need for environmental protection in all deep-sea mining activities.

3. The future of exploration

3.1. Standard exploration techniques

Surface-ship exploration techniques based on detecting discharge from active venting presently fall into two categories: one-dimensional, full-water-column profiles; and two-dimensional, near-bottom surveying. In either case, instrument packages range from a single self-contained sensor to a full instrument package such as a Conductivity-Temperature-Depth (CTD) system interfaced with sensors and sampling bottles (Baker et al., 1995). Plumes are standardly detected by hydrographic anomalies, such as changes in the potential temperature/salinity ratio, and, with more precision and spatial range, by optical anomalies, either light scattering or transmission.

A basic sampling strategy is simply vertical casts, widely (several kilometers) spaced along a ridge axis (German et al., 2006) or, on arcs, over the summits of discrete volcanic edifices (de Ronde et al., 2007) (Fig. 10). Such surveys account for ~80% of all vent fields discovered by plume detection. An efficient strategy for many investigations is combining plume detection with other over-the-side wire operations, such as adding MAPRs to rock coring and dredging wires (e.g., Scheirer et al., 1998; Edmonds et al., 2003; German et al., 2006). Although this strategy is common because it costs little in additional ship time, plumes from smaller vent fields can be easily missed.

Because hydrothermal plumes are dynamic features and vents are irregularly spaced, comprehensive exploration requires a spatially continuous two-dimensional survey (Fig. 11a). Most common are "tow-yos," where a CTD package is continually raised and lowered through a plume while slowly steaming along a track line (Baker et al., 1985) (Fig. 11b). Alternatively, plume sensors (such as MAPRs) can be arrayed along a tow cable as an instrument such as a side-scan sonar is towed at a fixed altitude above the seafloor (German et al., 1998) (Fig. 11c). In either case, the maximum tow speed is ~4 km/hr. An emerging trend in spatially continuous exploration is long-range Autonomous Underwater Vehicles (AUVs). For decades, AUVs have successfully accomplished detailed operations in limited areas while attended by a surface ship (German et al., 2008, Baker et al., 2012), but truly long-range operations have been challenging. One success is a 2013 expedition to the southern MAR, where the AUV ABYSS discovered 11 new plume fields by cruising 16 ridge segments between 13° and 33°S, covering >100 km on each dive for a total of 1161 km (Petersen et al., 2013). Another novel methodology is remote detection of hydrothermal bubble plumes using multibeam sonar on a surface ship. Chadwick et al. (2014) observed plumes of CO_2 bubbles rising from the 560-m-deep summit of an erupting

volcano on the Mariana arc. Temporal variability in plume height and volume imply that this technique could be used to monitor the level of eruptive activity.

3.2. "Best practices" exploration

Decades of standard exploration, primarily focused on high-temperature venting, have fashioned a "common knowledge" that tens to hundreds of kilometers separate vent fields (Edmonds, 2010; Hannington et al., 2014; Beaulieu et al., 2015). This view is fostered by survey techniques that are discontinuous, overlook isolated diffuse flow, and undercount closely spaced sites. "Best practices" exploration incorporates improved technology to overcome these shortcomings.

Interest in low-temperature diffuse flow fields, especially those isolated from high-temperature fields, has recently accelerated. New results from venting hosted in magma-dominated crust indicate that Fe, a biologically limiting nutrient in many oceanic regions, may be preferentially supplied to the ocean interior by low-temperature diffuse flow (German et al., 2015). Diffuse flow is ubiquitous around high-temperature fields but scarcely known elsewhere (Rose Garden, the first hydrothermal field discovered (Corliss et al., 1979), is a rare example). On slow-spreading ridge segments where magma is uncommon but mantle peridotites are exposed, vent fields can be essentially devoid of metals but rich in biologically active CH_4 and H_2 (Larson et al., 2015). Such fields, e.g., Lost City (Kelley et al., 2001), may be common but are almost immune to detection by optical or thermal sensors.

High-temperature fields are readily discoverable using widely dispersing particle-rich plumes, but the quasi-conservative nature of these plumes can also mask the true inventory of clustered fields that produce comingled plumes. A classic example is the Endeavour segment of the Juan de Fuca Ridge, where various exploration efforts, including many plume mapping operations, have occurred almost annually since the early 1980s (Kelley et al., 2012). At least eight active fields populate only 15 km of the axis, but it took more than two decades (1982–2005) to identify all these fields! Discriminating among clustered fields is not merely an accounting effort but is vital for understanding processes such as the circulation of crustal fluids in the shallow crust.

A solution to these exploration shortcomings is to add sensor capability to detect highly ephemeral tracers emitted by vents of all temperatures. Oxidation-Reduction Potential (ORP, sometimes called Eh) sensors have been used since the mid-1990s to identify hydrothermal discharge (e.g., Henry et al., 2002), but have seldom been used as a systematic exploration tool. ORP is sensitive to hydrothermal discharge at all temperatures because it detects even minute concentrations of reduced hydrothermal chemicals (e.g., Fe^{2+}, HS^-, H_2) that are out of equilibrium with the oxidizing ocean (Nakamura et al., 2000; Walker et al., 2007). Because these chemicals rapidly oxidize or metabolize close (~1 km (Stranne et al., 2010)) to their seafloor source, ORP signals provide a high-resolution measurement of vent-field distribution that discriminates among closely spaced sources. There is a pressing need for deep-sea real-time sensors that can quantitatively measure hydrothermal tracers such as Mn, Fe, and CH_4. Such sensors were developed long ago (Johnson et al., 1986; Massoth et al., 1998) but have proved overly complex and impractical to date.

3.3. Examples of "best practices" surveys

In this section I describe results from "best practices" surveys at four locations, two on MORs, one on a BASC, and one on a large arc volcano (Table 2). For each of the OSR sections I compare the vent field distribution given in the InterRidge Database to that determined by recent spatially continuous surveys using turbidity and ORP sensors. At the EPR ridge section we also compare these most recent data to "ground-truthing" by intensive camera tows in the same area. The four surveys were accomplished using a variety of methods: horizontal tow using ORP-equipped MAPRs attached to the tow cable of a ROV, horizontal tow with an ORP sensor on a side-scan sonar vehicle, CTD tow-yo, and sensors embedded in the AUV ABE. Baker et al. (2016) provide the detailed data analyses by which the inferred fields on the OSR segments were determined. In each case plume anomalies closer than 1 km are grouped as a single vent field. This precision is comparable to that achieved by AUVs mapping ORP anomalies in neutrally buoyant plumes during tightly gridded surveys (e.g., German et al., 2008).

3.3.1. East Pacific Rise, 9°–10°N

The EPR 9°–10°N is a fast-spreading (~110 mm/yr), first-order segment that ranks among the most studied of the global OSR system (Fornari et al., 2012). Numerous camera tows and dozens of submersible and ROV dives have scrutinized the area since the 1980s. The InterRidge Database lists eight vent fields; several encompass multiple discharge sources (chimneys and diffuse flow) within short ridge lengths (≤~1 km). In 2011, the segment was surveyed from 9.06° to 10.03°N (~110 km) with MAPRs attached to the JASON ROV at nominal altitudes of 45 m and 60 m above bottom during a single along-axis tow (Fig. 12) (Baker et al., 2016). The combination of 24 optical and 23 ORP anomalies identified 27 distinct fields (i.e., separated by >1 km). The F_s is thus 24.5, almost four times higher than the value of 7.3 estimated from the InterRidge Database. Fields with combined optical and ORP anomalies are considered high-temperature, whereas those with ORP alone (or predominant) are likely to be diffuse flow.

Support for a high concentration of vent fields on this segment comes from extensive and thorough seafloor visual surveys (>40% coverage within 100 m of the ridge axis itself) conducted in 1989 (Haymon et al., 1991; Haymon and White, 2004) (Fig. 12c). Between 9.15° and 9.9°N, indications of active venting were observed on camera tows in 38 of 90 intervals of 0.0083° (0.5´) latitude (interval length = 0.93 km, which approximates the 1 km plume resolution). These observations lead to F_s = 39, comparable to our estimate of 24.5. Another example comes from the southern EPR between 17.25° and 18.67°S (spreading rate = 150 mm/yr). Inventories from camera tows there (O'Neill, 1998; Haymon and White, 2004) identified active venting in 56 of 162 intervals of 0.0083° latitude (0.95 km), equivalent to an F_s = 36.

3.3.2. Eastern Galápagos Spreading Center, 85.7°–91°W

The intermediate-rate (~60 mm/yr), 520-km-long eastern GSC was the site of the first vent field discovered, Rose Garden at 86°W (Corliss et al., 1979), but no systematic hydrothermal surveys of this ridge section were undertaken until 2005/06 (Baker et al., 2008b) and 2011 (Shank et al., 2012). Based on four data sets—the original Rose Garden discovery, the partial 2005/06 survey that used a single ORP sensor on a side-scan sonar vehicle, optical plume data from a CTD tow-yo (Shank et al., 2012), and visual observations in 2002 (Shank et al.,

2003) and 2011 (Shank et al., 2012)—the InterRidge Database lists only seven fields (Fig. 13). Detailed analyses of the ORP data from 2005 and 2011 found 38 ORP and 14 light back-scattering (LBS) anomalies identifying 29 distinct vent fields. Thus, the F_s value increases from 0.7 using the InterRidge Database to 5.6.

The eastern GSC provides a good example of how ORP data can discriminate separate vent fields from a single combined optical plume. A uniform optical plume centered near 88.3°W extends >40 km along axis, whereas robust ORP anomalies pinpoint the location of three individual fields beneath the optical plume.

3.3.3. Eastern Lau Spreading Center, 19°–23°S

As noted in Section *2.1*, both concentrated exploration activity and geologic setting along a 420 km stretch of the ELSC apparently contribute to an unusually high number of active fields (31) in the InterRidge Database. Baker et al. (2016) re-analyzed ORP and LBS data from the two most areally complete surveys, which collected data from 19.3° to 22.8°S in 2004 along two parallel track lines, nominally ~600 m apart (Martinez et al., 2006). Plume data were collected by a single ORP sensor on a side-scan sonar ~120 m above bottom and LBS sensors arrayed along the towline (Fig. 14). These surveys found 175 ORP and 54 LBS anomalies that identify 96 fields, leading to F_s = 22.8, three times the InterRidge value of 8.

3.3.4. Brothers Volcano, Kermadec arc, 35°S

This survey exemplifies a different aspect of exploration, the scrutiny of a confined portion of seafloor by methods that correspond to the traditional terrestrial approach of geological mapping on a human scale. The summit caldera of Brothers Volcano is roughly 3 km in diameter, with a rim depth of ~1500 m and a floor depth exceeding 1850 m (Fig. 15a). Within the caldera, a large cone rises to 1200 m. Camera tows, dredges, plume surveys, and submersible operations during seven cruises from 1996 to 2005 provided powerful evidence of abundant venting, but plume patchiness and very limited visual data frustrated any ability to identify the location of all seafloor sources (de Ronde et al., 2011). In 2007 and 2011, however, the AUV ABE needed a mere 118 hr of survey time to map the fine-scale distribution of near-bottom (~50

m altitude) hydrothermal plumes throughout the entire caldera, compiling a detailed view of the caldera-wide distribution and nature of seafloor venting (Baker et al., 2012).

Sensors on ABE simultaneously measured hydrothermal plume anomalies in temperature, LBS, and ORP every 2–3 m along tracks separated by ~50 m horizontally, covering the entire caldera wall and floor (Fig. 15a). Systematic variations in the LBS/temperature ratio, combined with the location of ORP anomalies (Fig.15b), mapped the location of different types of fluid discharge (Fig. 15c). This program demonstrated that advanced deep-sea survey techniques using AUVs is an indispensable and cost-effective tool for acquiring a comprehensive understanding of the relationship between hydrothermal venting and geology on individual volcanoes and vent-field-sized areas on OSRs.

3.4. A new view of vent field spatial frequency

Adding the results from these ridge sections to the plot of existing F_s vs. u_s data yields a radically different alternative for the population of active vent fields (Fig. 16). If these new results are representative of all fast-spreading ridges—still a speculative hypothesis—such ridges may have vent populations perhaps much higher than currently assumed. Moreover, isolated ORP-only fields were surprisingly common, making up ~25% of observed fields on these sections. However, no conclusion about a true global inventory can be reached without further exploration on slow-spreading ridges, which include ~45% of the presently predicted global inventory of vent fields (Fig. 6). Exploration on slow ridges is impeded both by the vast expanse of available exploration areas and the complexity of the geology. Although the axial length of slow ridges compares with fast ridges, the width and depth of the axial valleys makes the area available for vent creation, and thus requiring exploration, at least an order of magnitude greater. The great abundance of mantle rocks exposed on slow ridges, and the likelihood of abundant vent fields populating those rocks (e.g., Kelley et al., 2001; Escartin et al., 2008; Connelly et al., 2012; German et al., 2016), augurs well for accelerating discoveries on the slow half of the global OSR system.

4. Some consequences of an expanded vent field population

These new results have implications more far-reaching than just improved accounting. For many chemical and geological processes, the spatial distribution of vent fields is a key variable. In the following sections I discuss some consequences of a seafloor vent field population that is greater and more closely spaced than the present "common knowledge" permits.

4.1. Hydrothermal circulation in the shallow crust

The location of seafloor discharge provides our only direct information on the distribution of hydrothermal upflow sites, and thus on the pattern of hydrothermal circulation in the shallow crust. Recent high-resolution, three-dimensional circulation models for hydrothermal fluids in the shallow crust of fast-spreading ridges (e.g., Hasenclever et al., 2014) provide simulations that support a much closer spacing of vent fields than inferred strictly from the InterRidge Database. These models yield a vent field spacing on the order of ~1 km, comparable to new observations on the fast-spreading EPR and ELSC (Fig. 16). The agreement improves further if we consider the modal vent spacing on those ridges, which is 2 km in each case (Baker et al., 2016). Caution is called for in transferring the model results to the real world, as the models assume uniform permeability along axis and a constant heat flux. Geological complications such as faults, varying rock types, and punctuated heat sources provided by episodic eruptions remain unaddressed. These variations no doubt contribute to the irregularity in vent field distributions apparent in detailed surveys (Figs. 12–14). The Hasenclever et al. (2014) model also predicts an increased spacing as the heat source (a melt lens) becomes deeper. This effect may play a role in the higher vent field spacing seen on the central GSC, where the melt lens (Detrick et al., 2002) is ~1 km deeper than on along the northern EPR (Carbotte et al., 2013).

It is instructive here to reconsider the Hannington et al. (2014) justification for a typical high-temperature field spacing of 50–100 km. They noted that to account for the high-temperature portion of the global hydrothermal heat flux (~10% of ~2×10^{12} W (Elderfield and Schultz, 1996)), some 50,000–100,000 individual black smokers are needed, each belching 2–5 MW. This combination could be satisfied with ~1 smoker every kilometer along OSRs, or a 100-smoker field every 50–100 km. But single-smoker sites are not uniformly arrayed along the

global OSR, and 100-smoker fields are not common. A more realistic (though still highly schematic) arrangement of 4-smoker fields every 2–4 km on fast ridges and 50-smoker fields every 25–50 km on slow ridges would also satisfy the global high-temperature heat flux requirement. Such an arrangement follows the presently known trend of vent field heat flux (245±170 MW on fast ridges to 1669±1354 MW on slow ridges (Baker, 2007)), though these averages come from a small data suite (n = 12 sites, some measured several times).

4.2. Global geochemical budgets

A long-standing principal in hydrothermal chemistry held that hydrothermal Fe little affects ocean chemistry, despite equaling or exceeding the riverine Fe flux (Elderfield and Schultz, 1996), because hydrothermal Fe was thought to be quickly and efficiently removed from the water column by precipitation and deposition (Johnson et al., 1997). This view began to change with the discovery that diffuse fluids can be rich in organic ligands capable of stabilizing dissolved hydrothermal metals (Sander et al., 2007).

Recent observations and modeling demonstrates the importance of this discovery. Sampling transects across the Atlantic (Saito et al., 2013) and the Pacific (Resing et al., 2015) show that previously unknown plumes of dissolved Fe, coincident with the known plumes of ^{3}He, can be traced for thousands of kilometers. These observations validate a recent modeling exercise explaining how diffuse fluids entrained into high-temperature discharge could provide a majority of the hydrothermal Fe injected into the interior of the deep ocean (German et al., 2015). Diffuse flow fields not associated with high-temperature discharge, such as discovered on the ridge sections in Figs. 12–14, were not considered in this model, so the model results are likely a minimum estimate of the hydrothermal Fe supply. Some of this previously unconsidered Fe is ultimately supplied to the iron-deficient surface waters of the Southern Ocean, where models estimate that it supports 15% to 30% of the export carbon production south of the Polar Front (Resing et al., 2015).

4.3. Resources

The commercial utilization of SMSs has been envisioned almost since the discovery of hydrothermal venting (e.g., Scott, 1987), and mining exploration has been active since at least 2000 (see Section *2.3.*). This effort proceeds even in the face of controversy about the true size of the resource. Diametrically opposite views on the magnitude of recoverable volcanogenic metals have been articulated by Cathles (2011), on one hand, and Hannington (2011) and Hannington et al. (2014) on the other. Cathles (2011) argues that this resource is effectively limitless; ~530 Gt, more than 600× greater than current reserves of terrestrial Cu+Zn. Recovery of almost all (>~99.5%) of this resource is presently inconceivable, as it would require mining the upper crust of the entire ocean floor. Hannington and colleagues respond that known minable SMSs on the neovolcanic zones of OSRs and arc volcanoes offer a Cu+Zn reservoir little larger than a single year of terrestrial production (~30 Mt/yr).

Here I address only how the issues discussed in this paper might affect the estimates of Hannington and colleagues. Hannington et al. (2014) used the distribution of known SMSs (>100 m^2 area) to project the full ocean inventory of minable (under present technology) deposits. The known distribution is strongly dependent on the exploration techniques discussed in this paper, and are thus subject to the same inadequacies. The absence of ORP data in most existing exploration results does not severely limit the discovery of actively forming SMS fields, since accumulation requires high-temperature vents that generate robust LBS plumes. However, even large fields can be missed using the most common standard exploration strategy—widely separated vertical casts—so the existing SMS database must be a minimum value. ORP anomalies might identify sites no longer accumulating SMS deposits but still venting low-temperature fluids. A prominent example is the sulfide deposits at 86.15°W on the GSC (Embley et al., 1988). ORP anomalies may also aid the discovery of sediment-hosted fields where the preponderance of metals is captured before fluids reach the seafloor (Campbell et al., 1994).

Other exploration-related uncertainties also affect the Hannington et al. (2014) analysis. Of the 32 control areas used by Hannington et al. (2014) to assess global SMS deposits, only one is on an ultraslow-spreading ridge. Each control area is assumed to be fully explored and representative of its spreading rate. These assumptions crucially apply to ultraslow ridges (<20 mm/yr), which total ~25% of global OSR length and account for fully ~50% of the current estimated SMS tonnage, but may not hold if vent fields occur on ultraslow-spreading ridges more often than predicted by the global spreading-rate trend (Fig. 5). Recent discoveries on

ultraslow ridges of vent fields hosted on both ultramafic rocks (Fouquet et al., 2010, and references within) and volcanic ridges (Pedersen et al., 2010; Tao et al., 2012; Kinsey and German, 2013) support this cautionary proposition.

An emerging, but potentially vital, resource potential is natural-product-based drugs from vent-associated microbes (Thornburg et al., 2010). Biotechnology companies have focused on investigating both whole cell thermophilic organisms and new enzymes for purposes as diverse as waste management, agriculture, biotechnology, cosmetics, pharmaceutics, and even bone healing. Most of the microbes used in these studies grow preferentially in low-temperature environments. Thus, the possibility of a substantial inventory of low-temperature-only fields, previously unrecognized, broadens the microbial population that may be biologically beneficial.

5. Conclusions

The number and spacing of hydrothermal discharge sites on the 93,000 km of ocean spreading ridges and submarine volcanic arcs is a key variable in understanding many chemical, biological, and physical processes occurring at the seafloor. Thirty-five years of vent field discovery has been remarkably steady at ~20/yr, yielding an inventory of >630 active discharge sites. About 80% of these sites are on ocean ridges, and the spatial frequency of these sites is currently predicted to be ~0.5–5/100 km of ridge crest. On volcanic arcs, the frequency ranges from ~0.9–1.8/100 km of arc length. Because of intensive exploration in the western Pacific since 2000, over 60% of all known vents now occur in national Exclusive Economic Zones.

Standard exploration techniques overwhelmingly rely on discontinuous sampling of hydrothermal plumes (vertical profiles separated by several kilometers) using optical sensors sensitive only to dispersing plumes of hydrothermal particles from high-temperature venting. Recent discoveries using continuous sampling (sensors towed behind a surface ship) and a sensor sensitive to reduced chemicals (e.g., Fe^{2+}, HS^-, H_2) from venting at all temperatures imply that the “common knowledge” of vent field frequency, on fast-spreading ridges, may be too low by a factor of ~3–6. This increase includes the observation that ~25% of all detected sites are apparently low-temperature, particle-poor venting resistant to discovery using optical sensors and discontinuous sampling. Remarkably, these results are consistent with comprehensive observations made decades ago by camera and submersible observations on a few ridge sections.

Elevated vent frequencies offer new quantitative constraints for models of seafloor processes such as hydrothermal circulation in the shallow crust, global geochemical budgets, and mineral and bioactive seafloor resources. Similar exploration techniques have not yet been widely employed on slow-spreading ridges, which account for half of all ridge length. The broad cross-section of those ridges, combined with multiple possible heat sources (magma, cooling mantle rocks, serpentinization), offer both an exploration challenge and the opportunity of abundant sites of past and present venting.

Acknowledgements

This research was supported by the NOAA/PMEL Earth-Ocean Interactions Program and the Joint Institute for the Study of the Atmosphere and Ocean (JISAO) under NOAA Cooperative Agreement No. NA10OAR4320148. PMEL contribution 4511, JIASO contribution 2017-068.

References

Achterberg, E.P., Moore, C.M., Henson, S.A., Steigenberger, S., Stohl, A., Eckhardt, S., Avendano, L.C., Cassidy, M., Hembury, D., Klar, J.K., Lucas, M.I., Macey, A.I., Marsay, C.M., Ryan-Keogh, T.J., 2013. Natural iron fertilization by the Eyjafjallajökull volcanic eruption. Geophys. Res. Lett. 40(5), 921-926, doi:10.1002/grl.50221.

Baker, E.T., 2007. Hydrothermal cooling of midocean ridge axes: Do measured and modeled heat fluxes agree?. Earth Planet. Sci. Lett. 263(1–2), 140–150.

Baker, E.T., German, C.R., 2004. On the global distribution of hydrothermal vent fields. In: German, C.R., Lin, J., Parson, L.M. (Eds.), Mid-Ocean Ridges: Hydrothermal Interactions Between the Lithosphere and Oceans. Geophys. Monogr. Ser. 148, AGU, Washington, D.C. pp. 245–266.

Baker, E.T., Hammond, S.R., 1992. Hydrothermal venting and the apparent magmatic budget of the Juan de Fuca Ridge. J. Geophys. Res. 97, 3443–3456.

Baker, E.T., Lavelle, J.W., Massoth, G.J.,1985. Hydrothermal particle plumes over the southern Juan de Fuca Ridge. Nature 316, 342–344.

Baker, E.T., German, C.R., Elderfield, H., 1995. Hydrothermal plumes over spreading-center axes: Global distributions and geological inferences. In: Humphris, S., Zierenberg, R., Mullineaux, L.S., Thomson, R. (Eds.), Seafloor Hydrothermal Systems: Physical, Chemical, Biological, and Geological Interactions. Geophys. Monogr. Ser. 91, AGU, Washington D.C., pp. 47–71.

Baker, E.T., Chen, Y.J., Phipps Morgan, J., 1996. The relationship between near-axis hydrothermal cooling and the spreading rate of midocean ridges. Earth Plan. Sci. Lett. 142, 137–145.

Baker, E.T., Hey, R.N., Lupton, J.E., Resing, J.A., Feely, R.A., Gharib, J.J., Massoth, G.J., Sansone, F.J., Kleinrock, M., Martinez, F., Naar, D.F., Rodrigo, C., Bohnenstiehl, D., Pardee, D., 2002. Hydrothermal venting along Earth's fastest spreading center: East Pacific Rise, 27.5°– 32.3°S. J. Geophys. Res. 107(B7), 2130, doi:10.1029/2001JB000651.

Baker, E.T., Embley, R.W., Walker, S.L., Resing, J.A., Lupton, J.E., Nakamura, K., de Ronde, C.E.J., Massoth, G.J., 2008a. Hydrothermal activity and volcano distribution along the Mariana arc. J. Geophys. Res. 113, B08S09, doi:10.1029/2007JB005423.

Baker, E.T., Haymon, R.M., Resing, J.A., White, S.M., Walker, S.L., Macdonald, K.C., Nakamura, K., 2008b. High-resolution surveys along the hot spot–affected Galápagos Spreading Center: 1. Distribution of hydrothermal activity, Geochem. Geophys. Geosyst. 9, Q09003, doi:10.1029/2008GC002028.

Baker, E.T., Walker, S.L., Embley, R.W., de Ronde, C.E.J., 2012. High-resolution hydrothermal mapping of Brothers caldera, Kermadec arc. Econ. Geol. 107, 1583–1593, doi:10.2113/econgeo.107.8.1583.

Baker, E.T., Resing, J.A., Haymon, R.M., Tunnicliffe, V., Lavelle, J.W., Martinez, F., Ferrini, V., Walker, S.L., Nakamura, K., 2016. How many vent fields?. New estimates of vent field populations on ocean ridges from precise mapping of hydrothermal discharge locations. Earth Planet. Sci. Lett. 449, 186–196, doi:10.1016/j.epsl.2016.05.031.

Ballard, R.D., Hekinian, R., Francheteau, J., 1984. Geological setting of hydrothermal activity at 12°50´N on the East Pacific Rise: A submersible study. Earth Planet. Sci. Lett. 69(1), 176–186.

Beaulieu, S.E., Baker, E.T., German, C.R., Maffei, A., 2013. An authoritative global database for active submarine hydrothermal vent fields. Geochem. Geophys. Geosyst. 14, 4892–4905, doi:10.1002/2013GC004998.

Beaulieu, S.E., Baker, E.T., German, C.R., 2015. Where are the undiscovered vents on oceanic spreading ridges?. Deep-Sea Res. Pt. II 121, 202–212, doi:10.1016/j.dsr2.2015.05.001.

Bird, P., 2003. An updated digital model of plate boundaries. Geochem. Geophys. Geosyst. 4(3), 1027, doi:10.1029/2001GC000252.

Bischoff, J.L., Rosenbauer, R.J., 1984. The critical point and two-phase boundary of seawater, 200–500°C. Earth Planet. Sci. Lett. 68, 172–180.

Campbell, A.C., German, C.R., Palmer, M.R., Gamo, T., Edmond, J.M., 1994. Chemistry of hydrothermal fluids from the Escanaba Trough, Gorda Ridge. In: Morton, J.L., Zierenberg, R.A., Reiss, C.A. (Eds.), Geologic, Hydrothermal, and Biologic Studies at Escanaba Trough, Gorda Ridge, Offshore Northern California. U.S. Geol. Surv. Bull. 2022, pp.201–221.

Cannat, M., Cann, J., Maclennan, J., 2004. Some hard rock constraints on the supply of heat to mid-ocean ridges. In: , C., J., L. (Eds.), Mid-Ocean Ridges: Hydrothermal Interactions Between the Lithosphere and Oceans. Geophys. Monogr. Ser. 148, AGU, Washington, D.C., pp. 111–150.

Carbotte, S.M., Marjanović, M., Carton, H., Mutter, J.C., Canales, J.P., Nedimović, M.R., Han, S., Perfit, M.R., 2013. Fine-scale segmentation of the crustal magma reservoir beneath the East Pacific Rise. Nature Geosci. 6, 866–870, doi:10.1038/ngeo1933.

Cathles, L.M., 2011. What processes at mid-ocean ridges tell us about volcanogenic massive sulfide deposits. Miner. Depos. 46(5–6), 639–657, doi:10.1007/s00126-010-0292-9.

Chadwick, Jr., W.W., Merle, S.G., Buck, N.J., Lavelle, J.W., Resing, J.A., Ferrini, V., 2014. Imaging of CO_2 bubble plumes above an erupting submarine volcano, NW Rota-1, Mariana Arc. Geochem. Geophys. Geosyst. 15(11), 4325–4342, doi: 10.1002/2014GC005543.

Coale, K.H., Fitzwater, S.E., Gordon, R.M., Johnson, K.S., Barber, R.T., 1996. Control of community growth and export production by upwelled iron in the equatorial Pacific Ocean. Nature 379, 621–624.

Connelly, D.P., Copley, J.T., Murton, B.J., Stansfield, K., Tyler, P.A., German, C.R., Van Dover, C.L., Amon, D., Furlong, M., Grindlay, N., Hayman, N., Hühnerbach, V., Judge, M., Le Bas, T., McPhail, S., Meier, A., Nakamura, K., Nye, V., Pebody, M., Pedersen, R.B., Plouviez, S., Sands, C., Searle, R.C., Stevenson, P., Taws, S., Wilcox, S., 2012. Hydrothermal vent fields and chemosynthetic biota on the world's deepest seafloor spreading centre. Nature Commun. 3, 620, doi:10.1038/ncomms1636.

Corliss, J.B., Dymond, J., Gordon, L.I., Edmond, J.M., von Herzen, R.P., Ballard, R.D., Green, K., Williams, D., Bainbridge, A., Crane, K., van Andel, , 1979. Submarine thermal springs on the Galapagos Rift. Science 203, 1073–1083.

Craig, H., Clarke, W.B., Beg, M.A., 1975. Excess ^{3}He in deep water on the East Pacific Rise. Earth. Planet. Sci. Lett. 26, 125–132.

de Ronde, C.E.J., Baker, E.T., Massoth, G.J., Lupton, J.E., Wright, I.C., Feely, R.A., Greene, R.R., 2001. Intra-oceanic subduction-related hydrothermal venting, Kermadec volcanic arc, New Zealand. Earth Planet. Sci. Lett. 193, 359–369.

de Ronde, C.E.J., Massoth, G.J., Baker, E.T., Lupton, J.E., 2003. Submarine hydrothermal venting related to volcanic arcs, Giggenbach Memorial Volume. In: Simmons, S.F., Graham, I. (Eds.), Volcanic, Geothermal and Ore-forming Fluids: Rulers and Witnesses of Processes Within the Earth. Special Publication 10, The Geochemical Society, Washington, D.C., pp. 91–110.

de Ronde, C.E.J., Baker, E.T., Massoth, G.J., Lupton, J.E., Wright, I.C., Sparks, R.J., Bannister, S.C., Reyners, M.E., Walker, S.L., Greene, R.R., Ishibashi, J., Faure, K., Resing, J.A., Lebon, G.T., 2007. Submarine hydrothermal activity along the mid-Kermadec Arc, New Zealand: Large-scale effects on venting. Geochem. Geophys. Geosyst. 8, Q07007, doi:10.1029/2006GC001495.

de Ronde, C.E.J., Massoth, G.J., Butterfield, D.A., Christenson, B.W., Ishibashi, J., Ditchburn, R.G., Hannington, M.D., Brathwaite, R.L., Lupton, J.E., Kamenetsky, V.S., Graham, I.J., Zellmer, G.F., Dziak, R.P., Embley, R.W., Dekov, V.M., Munnik, F., Lahr, J., Evans, L.J., Takai, K., 2011. Submarine hydrothermal activity and gold-rich mineralization at Brothers volcano, Kermadec arc, New Zealand. Miner. Depos. 46, 541–584, doi:10.1007/s00126-011-0345-8.

Detrick, R.S., Sinton, J.M., Ito, G., Canales, J.P., Behn, M., Blacic, T., Cushman, B., Dixon, J.E., Graham, D.W., Mahoney, J.J., 2002. Correlated geophysical, geochemical, and volcanological manifestations of plume-ridge interaction along the Galápagos Spreading Center. Geochem. Geophys. Geosyst. 3, 8501, doi:10.1029/2002GC000350.

Edmonds, H.N., 2010. Chemical signatures from hydrothermal venting on slow spreading ridges. In: Rona, P.A., Devey, C.W., Dyment, J., Murton, B. (Eds.), Diversity of Hydrothermal Systems on Slow Spreading Ocean Ridges. Geophys. Monogr. Ser. 188. AGU, Washington D.C., pp. 27–42.

Edmonds, H.N., Michael, P.J., Baker, E.T., Connelly, D.P., Snow, J.E., Langmuir, C.H., Dick, H.J.B., Mühe, R., German, C.R., Graham, D.W., 2003. Discovery of abundant hydrothermal venting on the ultraslow-spreading Gakkel Ridge in the Arctic Ocean. Nature 421, 252–256, doi:10.1038/nature01351.

Elderfield, H., Schultz, A., 1996. Mid-ocean ridge hydrothermal fluxes and the chemical composition of the ocean. Annu. Rev. Earth Planet. Sci. 24, 191–224, doi:10.1146/annurev.earth.24.1.191.

Embley, R.W., Jonasson, I.R., Perfit, M.R., Franklin, J.M., Tivey, M.A., Malahoff, A., Smith, M.F., Francis, T.J.G., 1988. Submersible investigation of an extinct hydrothermal system on the Galapagos Ridge: Sulfide mounds, stockwork zone, and differentiated lavas. Can. Mineral. 26(3), 517–539.

Embley, R.W., Baker, E.T., Butterfield, D.A., Chadwick Jr., W.W., Lupton, J.E., Resing, J.A., de Ronde, C.E.J., Nakamura, K., Tunnicliffe, V., Dower, J.F., Merle, S.G., 2007. Exploring the submarine ring of fire: Mariana Arc—Western Pacific. Oceanography 20(4), 68–79, doi:10.5670/oceanog.2007.07.

Escartin, J., Smith, D.K., Cann, J., Schouten, H., Langmuir, C.H., Escrig, S., 2008. Central role of detachment faults in accretion of slow-spreading oceanic lithosphere. Nature 455(7214), 790–794, doi:10.1038/nature07333.

Fornari, D.J., Von Damm, K.L., Bryce, J.G., Cowen, J.P., Ferrini, V., Fundis, A., Lilley, M.D., Luther III, G.W., Mullineaux, L.S., Perfit, M.R., Meana-Prado, M.F., Rubin, K.H., Seyfried Jr., W.E., Shank, T.M., Soule, S.A., Tolstoy, M., White, S.M., 2012. The East Pacific Rise between 9°N and 10°N: Twenty-five years of integrated, multidisciplinary

oceanic spreading center studies. Oceanography 25, 18–43, doi:10.5670/oceanog.2012.02.

Fouquet, Y., Cambon, P., Etoubleau, J., Charlou, J.L., Ondreas, H., Barriga, F.J.A.S., Cherkashov, G., Semkova, T., Poroshina, I., Bohn, M., Donval, J.P., Henry, K., Murphy, P., Rouxel, O., 2010. Geodiversity of hydrothermal processes along the Mid-Atlantic Ridge and ultramafic-hosted mineralization: A new type of oceanic Cu–Zn–Co–Au volcanogenic massive sulfide deposit. In: Rona, P.A., Devey, C.W., Dyment, J., Murton, B.J. (Eds.), Diversity of Hydrothermal Systems on Slow Spreading Ocean Ridges. Geophys. Monogr. 188, AGU, Washington, D.C., pp. 297–320.

German, C.R., Parson, L.M., 1996. Hydrothermal exploration at the Azores Triple-Junction: Tectonic control of venting at slow-spreading ridges?. Earth Planet. Sci. Lett. 138, 93–104.

German, C.R., Baker, E.T., Mevel, C., Tamaki, K., the FUJI Scientific Team, 1998. Hydrothermal activity along the southwest Indian Ridge. Nature 395, 490–493.

German, C.R., Baker, E.T., Connelly, D.P., Lupton, J.E., Resing, J., Prien, R.D., Walker, S.L., Edmonds, H.N., Langmuir, C.H., 2006. Hydrothermal exploration of the Fonualei Rift and Spreading Center and the Northeast Lau Spreading Center. Geochem. Geophys. Geosyst. 7, Q11022, doi:10.1029/2006GC001324.

German, C.R., Yoerger, D.R., Jakuba, M., Shank, T.M., Langmuir, C.H., Nakamura, K.I., 2008. Hydrothermal exploration with the autonomous benthic explorer. Deep-Sea Res. Part I-Oceanogr. Res. Pap. 55(2), 203–219, doi:10.1016/j.dsr.2007.11.004.

German, C.R., Legendre, L.L., Sander, S.G., Niquil, N., Luther III, G.W., Bharati, L., Han, X., Le Bris, N., 2015. Hydrothermal Fe cycling and deep ocean organic carbon scavenging: Model-based evidence for significant POC supply to seafloor sediments. Earth Planet. Sci. Lett. 419, 143–153, doi:10.1016/j.epsl.2015.03.012.

German, C.R., Petersen, S., Hannington, M.D., 2016. Hydrothermal exploration of mid-ocean ridges: Where might the largest sulfide deposits be forming?. Chem. Geol. 420, 114–126, doi:10.1016/j.chemgeo.2015.11.006.

Gràcia, E., Charlou, J.L., Radford-Knoery, J., Parson, L.M., 2000. Non-transform offsets along the Mid-Atlantic Ridge south of the Azores (38°N–34°N): Ultramafic exposures and hosting of hydrothermal vents. Earth Planet. Sci. Lett. 177, 89–103.

Hammond, S.R., Embley, R.W., Baker, E.T., 2015. The NOAA Vents Program 1983 to 2013: Thirty years of ocean exploration and research. Oceanography 28, 160–173, doi.org/ 10.5670/ oceanog.2015.17.

Hannington, M., 2011. Comments on "What processes at mid-ocean ridges tell us about volcanogenic massive sulfide deposits" by L.M. Cathles. Miner. Depos. 46, 659–663, doi:10.1007/s00126-011-0329-8.

Hannington, M., Jamieson, J., Monecke, T., Petersen, S., Beaulieu, S., 2014. The abundance of seafloor massive sulfide deposits. Geology 39, 1155–1158, doi:10.1130/G32468.1.

Hasenclever, J., Theissen-Krah, S., Rüpke, L.H., Morgan, J.P., Iyer, K., Petersen, S., Devey, C.W., 2014. Hybrid shallow on-axis and deep off-axis hydrothermal circulation at fast-spreading ridges. Nature 508, 508–512, doi:10.1038/nature13174.

Haymon, R.M., Fornari, D.J., Edwards, M.H., Carbotte, S., Wright, D., Macdonald, K.C., 1991. Hydrothermal vent distribution along the East Pacific Rise Crest (9°09´–54´N) and its relationship to magmatic and tectonic processes on fast-spreading mid-ocean ridges. Earth Planet. Sci. Lett. 104, 513–534.

Henry, P., Lallemant, S., Nakamura, K., Tsunogai, U., Mazzotti, S., Kobayashi, K., 2002. Surface expression of fluid venting at the toe of the Nankai wedge and implications for flow paths. Mar. Geol. 187(1), 119–143.

Husson, L., Conrad, C.P., 2012. On the location of hotspots in the framework of mantle convection. Geophys. Res. Lett. 39(17), L17304, doi:10.1029/2012GL052866.

Johnson, K.S., Beehler, C.L., Sakamoto-Arnold, C.M., Childress, J.J., 1986. In situ measurements of chemical distributions in a deep-sea hydrothermal vent field. Science 231(4742), 1139–1141.

Johnson, K.S., Gordon, R.M., Coale, K.H., 1997. What controls dissolved iron concentrations in the world ocean?. Mar. Chem. 57(3), 137–161.

Kelley, D.S., Karson, J.A., Blackman, D.K., Früh-Green, G.L., Butterfield, D.A., Lilley, M.D., Olson, E.J., Schrenk, M.O., Roe, K.K., Lebon, G.T., Rivizzigno, P., the AT3-60 Shipboard Party, 2001. An off-axis hydrothermal vent field near the Mid-Atlantic Ridge at 30°N. Nature 412(6843), 145–149, doi:10.1038/35084000.

Kelley, D.S., Baross, J.A., Delaney, J.R., 2002. Volcanoes, fluids, and life at mid-ocean ridge spreading centers. Annu. Rev. Earth Planet. Sci. 30(1), 385–491.

Kelley, D.S., Carbotte, S.M., Caress, D.W., Clague, D.A., Delaney, J.R., Gill, J.B., Hadaway, H., Holden, J.F., Hooft, E.E., Kellogg, J.P., Lilley, M.D., Stoermer, M., Toomey, D., Weekly, R., Wilcock, W.S.D., 2012. Endeavour Segment of the Juan de Fuca Ridge: One of the most remarkable places on Earth. Oceanography 25, 44–61, doi:10.5670/oceanog.2012.03.

Kim, J., Son, S.K., Son, J.-W., Kim, K.-H., Shim, W.J., Kim, C.H., Lee, K.-Y., 2009. Venting sites along the Fonualei and Northeast Lau Spreading Centers and evidence of hydrothermal activity at an off-axis caldera in the northeastern Lau Basin. Geochemical Journal, 43(1), 1–13, doi:10.2343/geochemj.0.0164.

Kinsey, J.C., German, C.R., 2013. Sustained, volcanically-hosted venting at an ultra-slow ridge: Piccard Hydrothermal Field, Mid-Cayman Rise. Earth Planet. Sci. Lett. 380, 162–168, doi:10.1016/j.epsl.2013.08.001.

Klinkhammer, G., Bender, M., Weiss, R.F., 1977. Hydrothermal manganese in the Galapagos Rift. Nature 269, 319–320, doi:10.1038/269319a0.

Knauss, J.A., 1962. On some aspects of the deep circulation of the Pacific. J. Geophys. Res. 67, 3943–3954.

Larson, B.I., Lang, S.Q., Lilley, M.D., Olson, E.J., Lupton, J.E., Nakamura, K., Buck, N.J., 2015. Stealth export of hydrogen and methane from a low temperature serpentinization system. Deep-Sea Res. Part II-Top. Stud. Oceanogr. 121, 233–245, doi:10.1016/j.dsr2.2015.05.007.

Lupton, J.E., Klinkhammer, G.P., Normark, W.R., Haymon, R., Macdonald, K.C., Weiss, R.F., Craig, H., 1980. Helium-3 and manganese at the 21°N East Pacific Rise hydrothermal site. Earth Planet. Sci. Lett. 50(1), 115–127.

Lupton, J., Butterfield, D., Lilley, M., Ishibashi, J., Hey, D., Evans, L., 1999. Gas chemistry of hydrothermal fluids along the East Pacific Rise, 5°S to 32°S. Eos Trans. AGU 80(46), Fall Meet. Suppl., F1099.

Macdonald, K., Fox, P.J., 1988. The axial summit graben and cross-sectional shape of the East Pacific Rise as indicators of axial magma chambers and recent volcanic eruptions. Earth Planet. Sci. Lett. 88, 119–131.

Martinez, F., Taylor, B., Baker, E.T., Resing, J.A., Walker, S.L., 2006. Opposing trends in crustal thickness and spreading rate along the back-arc Eastern Lau Spreading Center:

Implications for controls on ridge morphology, faulting, and hydrothermal activity. Earth Planet. Sci. Lett. 245, 655–672.

Massoth, G.J., Baker, E.T., Feely, R.A., Lupton, J.E., Collier, R.W., Gendron, J.F., Roe, K.K., Maenner, S.M. and Resing, J.A., 1998. Manganese and iron in hydrothermal plumes resulting from the 1996 Gorda Ridge Event. Deep-Sea Res. Part II-Top. Stud. Oceanogr. 45, 2683–2712.

Massoth, G.J., Baker, E.T., Worthington, T., Lupton, J.E., de Ronde, C., Arculus, R.A., Walker, S.L., Nakamura, K., Ishibashi, J.-I., Stoffers, P., Resing, J.A., Greene, R., Lebon, G., 2007. Multiple hydrothermal sources along the south Tonga arc and Valu Fa Ridge. Geochem. Geophys. Geosyst. 8(11), Q11008, doi:10.1029/2007GC001675.

McConachy, T.F., Ballard, R.D., Mottl, M.J., Von Herzen, R.P., 1986. Geologic form and setting of a hydrothermal vent field at lat 10°56´N, East Pacific Rise: A detailed study using *Angus* and *Alvin*. Geology 14(4), 295–298.

Miller, A.R., Densmore, C.D., Degens, E.T., Hathaway, J.C., Manheim, F.T., McFarlin, P.F., Pocklington, R., Jokela, A., 1966. Hot brines and recent iron deposits in deeps of the Red Sea. Geochim. Cosmochim. Acta 30(3), 341–359.

Nakamura, K., Veirs, S., Sarason, C.P., McDuff, R.E., Stahr, F., Yoerger, D.R., Bradley, A.M., 2000. Electrochemical signals in rising buoyant plumes and tidally oscillating plumes at the Main Endeavour vent field, Juan de Fuca Ridge [abs.]. EOS Trans. AGU 81(48), Fall Meet. Suppl., Abstract OS52I-05.

O'Neill, J.H., 1998. Geologic controls on distribution of hydrothermal vents on the superfast-spreading southern East Pacific Rise. Thesis Dissertation, University of California, Santa Barbara, 69 pp.

Pedersen, R.B., Rapp, H.T., Thorseth, I.H., Lilley, M.D., Barriga, F.J.A.S., Baumberger, T., Flesland, K., Fonseca, R., Früh-Green, G.L., Jorgensen, S.L., 2010. Discovery of a black smoker vent field and vent fauna at the Arctic Mid-Ocean Ridge. Nat. Commun. 1, 126, doi:10.1038/ncomms1124.

Petersen, S., Devey, C.W., Walter, M., Jamieson, J.W., Yeo, I., Nakamura, K., Rothenbeck, M., Steinführer, A., Triebe, L., 2013. AUV-based long-range exploration for hydrothermal activity between 13°-33°S along the Southern Mid-Atlantic Ridge. Recent Developments in Atlantic Seabed Minerals Exploration and Other Topics, UMI 2013, 42nd Underwater

Mining Institute Conference, Rio de Janeiro and Porto de Galinhas, Brazil, 21–29 October 2013.

Resing, J.A., Baker, E.T., Lupton, J.E., Walker, S.L., Butterfield, D.A., Massoth, G.J., Nakamura, K., 2009. Chemistry of hydrothermal plumes above submarine volcanoes of the Mariana Arc. Geochem. Geophys. Geosyst. 10(2), Q02009, doi:10.1029/2008GC002141.

Resing, J.A., Sedwick, P.N., German, C.R., Jenkins, W.J., Moffett, J.W., Sohst, B.M., Tagliabue, A., 2015. Basin-scale transport of hydrothermal dissolved metals across the South Pacific Ocean. Nature 523, 200–203, doi:10.1038/nature14577.

Rona, P.A., Devey, C.W., Dyment, J., Murton, B.J., 2010. Diversity of Hydrothermal Systems on Slow Spreading Ocean Ridges. Geophys. Monogr. Ser. 188. AGU, Washington, D.C.

Saito, M.A., Noble, A.E., Tagliabue, A., Goepfert, T.J., Lamborg, C.H., Jenkins, W.J., 2013. Slow-spreading submarine ridges in the South Atlantic as a significant oceanic iron source. Nature Geosci. 6(9), 775–779.

Sander, S.G., Koschinsky, A., Massoth, G., Stott, M., Hunter, K.A., 2007. Organic complexation of copper in deep-sea hydrothermal vent systems. Environ. Chem. 4, 81–89.

Scheirer, D.S., Baker, E.T., Johnson, K.T.M., 1998. Detection of hydrothermal plumes along the Southeast Indian Ridge near the Amsterdam-St. Paul hotspot. Geophys. Res. Lett. 25, 97–100.

Scott, S.D., 1987. Seafloor polymetallic sulfides: Scientific curiosities or mines of the future?. In: Teleki, P.G., Dobson, M.R., Moore, J.R., von Stackelberg, U. (Eds.), Marine Minerals: Advances in Research and Resource Assessment. NATO ASI 194, pp. 277–300.

Shank, T.M., Baker, E.T., Embley, R.W., Hammond, S., Holden, J.F., White, S., Walker, S.L., Calderón, M., Herrera, S., Lin, T.J., Munro, C., Heyl, T., Stewart, L.C., Malik, M., Lobecker, E., Potter, J., 2012. Exploration of the deepwater Galápagos region. In: Bell, K.L.C., Elliott, K., Martinez, C., Fuller, S.A. (Eds.), New Frontiers in Ocean Exploration: The E/V *Nautilus* and NOAA Ship *Okeanos Explorer* 2011 Field Season. Oceanography 25(Suppl.), 50–51.

Shank, T., Fornari, D., Yoerger, D., Humphris, S., Bradley, A., Hammond, S., Lupton, J., Scheirer, D., Collier, R., Reysenbach, A.L. and Ding, K., 2003. Deep submergence

synergy: Alvin and ABE explore the Galápagos Rift at 86 W. *Eos, Transactions American Geophysical Union*, *84*(41), pp.425-433.

Spiess, F.N., Macdonald, K.C., Atwater, T., Ballard, R., Carranza, A., Cordoba, D., Cox, C., Diaz Garcia, V.M., Francheteau, J., Guerrero, J., Hawkins, J., Haymon, R., Hessler, R., Juteau, T., Kastner, M., Larson, R., Luyendyk, B., Macdougall, J.D., Miller, S., Normark, W., Orcutt, J., Rangin, C., 1980. East Pacific Rise: Hot springs and geophysical experiments. Science 207(4438), 1421–1433.

Stranne, C., Sohn, R.A., Liljebladh, B., Nakamura, K.I., 2010. Analysis and modeling of hydrothermal plume data acquired from the 85°E segment of the Gakkel Ridge. J. Geophys. Res. Oceans 115(C6), C06028, doi:10.1029/2009JC005776.

Tao, C., Lin, J., Guo, S, Chen, Y.J., Wu, G., Han, X., German, C.R., Yoerger, D.R., Zhou, N., Li, H., Su, X., Zhu, J., DY115-19/DY115-20 Science Parties, 2012. First active hydrothermal vents on an ultraslow-spreading center: Southwest Indian Ridge. Geology 40, 47–50, doi:10.1130/G32389.1.

Thornburg, C.C., Zabriskie, T.M., McPhail, K.L., 2010. Deep-sea hydrothermal vents: Potential hot spots for natural products discovery?. J. Nat. Prod. 73(3), 489–499, doi:10.1021/np900662k.

VLIZ, 2009. Maritime Boundaries Geodatabase, World EEZ Version 5, Released 01.10.09. Available at: http://www.marineregions.org/downloads.php#eez.

Walker, S.L., Baker, E.T., Massoth, G.J., Hey, R.N., 2004. Short-term variations in the distribution of hydrothermal plumes along a superfast spreading center, East Pacific Rise, 27°30´–32°20´S. Geochem. Geophys. Geosyst. 5, Q12005, doi:10.1029/2004GC000789.

Walker, S.L., Baker, E.T., Resing, J.A., Nakamura, K., McLain, P.D., 2007. A new tool for detecting hydrothermal plumes: An ORP sensor for the PMEL MAPR [abs.]. EOS Trans. AGU 88(52), Fall Meet. Suppl., Abstract V21D-0753.

Zellmer, K.E., Taylor, B., 2001. A three-plate kinematic model for Lau Basin opening. Geochem. Geophys. Geosyst. 2(5), 1020, doi:10.1029/2000GC000106.

Fig. 1. (a) Jets of sulfur (~112°C) shooting out from holes in sediment-covered seafloor. Courtesy of MARUM, University of Bremen, and NOAA-PMEL. (b) Large chimneys, reaching 35-40 m in height, form close to each other at a depth of 1,555 m discharging fluids at ~250°C. Courtesy of MARUM, University of Bremen, and NOAA-PMEL. (c) 350°C fluids discharge from a black smoker. Courtesy NOAA Okeanos Explorer Program. (d) Riftia tubeworms colonize diffuse vent habitats between broken pieces of lava. Courtesy of NOAA Okeanos Explorer Program. (e) White flocculent mats in and around the extremely gassy, high-temperature (>100°C, 212°F) white smokers at Champagne Vent. Image courtesy of Submarine Ring of Fire 2004 Exploration, NOAA Vents Program. (f) A sampler gathers the top layer of a microbial mat discharging diffuse fluids (17°C). Courtesy of Submarine Ring of Fire 2014 - Ironman, NSF/NOAA, Jason, Copyright Woods Hole Oceanographic Institute.

Fig. 2. Global map of known (confirmed and inferred) vent fields discovered prior to 2000 (black squares) and afterward (black circles). Color of oceanic spreading ridges indicates spreading rate categorized to ultraslow (<20 mm/yr), slow (20–50 mm/yr), intermediate (50–80 mm/yr), fast (80–140 mm/yr), or superfast (>140 mm/yr, only present on the East Pacific Rise from ~15°–32°S, and mostly obscured by the vent field symbols). Other information includes plate boundaries (Bird, 2003), thin black lines; Exclusive Economic Zones (VLIZ, 2009), thin gray lines; and hotspots (Husson and Conrad, 2012), gray open stars. Figure adapted from Beaulieu et al. (2015).

Fig. 3. Yearly trend of vent field discovery since 1980, based on the InterRidge Database compilation. Note that an increase in the discovery rate on back-arc spreading centers (BASCs) and arcs from 2000 to 2010 led to a slowing of discovery on mid-ocean ridges (MORs) during that time. Linear least-squares regression fits to each data set give a discovery rate of ~10/yr on MORs and ~4/yr on BASCs and arcs (r >0.96 for each line).

Fig. 4. Relationships between OSR spreading rate (binned in 10 mm/yr increments) and vent field population. (a) Most known vent fields occur on slow-spreading OSRs (<55 mm/yr) because those ridges comprise ~60% of total ridge length. (b) The spatial frequency of known vent fields (F_s, fields/100 km) roughly increases with spreading rate, which is a proxy for the magmatic heat budget. These trends are significantly controlled by the degree of exploration

conducted in each spreading rate bin (colored bars in (a)). For example, low F_s values in the 110 and 130 mm/yr bins (b) correspond to a high percentage of unsurveyed ridge crest length (blue bars) compared to other fast-spreading ridges.

Fig. 5. Vent field spatial frequency, F_s, vs. spreading rate (u_s) for 27 OSR sections (red circles). A solid black line shows least-squares regression ($F_s = 0.81 + 0.024u_s$, $r = 0.53$) trend, with the ±95% confidence intervals of the slope shown by the grey curves. Binning the data by five spreading rate intervals (blue squares, bars show ±1 standard deviations) gives the same regression with a much-improved fit ($r = 0.96$). A least-squares fit forced through the origin (purple dashed line) shows a hypothetical trend ($F_s = 0.033u_s$) if vent fields were powered only by heat from axial magma chambers. See Tables 1 and 2 for details of each ridge section.

Fig. 6. The distribution of already discovered (red bars) and predicted (blue bars) OSR vent fields vs. spreading rate. Intervals where the ratio of predicted/discovered vents is low correspond to areas of concentrated exploration.

Fig. 7. The population of known (blue bars) and hydrothermally active (red bars) submarine volcanoes on arcs. Bold names indicate five intraoceanic arcs and regular type names indicate 16 island arcs. Intraoceanic arcs, where submarine volcanoes are common, have been explored more thoroughly than most island arcs. The Aeolian, Solomon, and TLTF (Tabar-Lihir-Tanga-Feni) arcs are the best explored island arcs for hydrothermal activity, while on several island arcs no submarine volcanoes have yet been identified.

Fig. 8. Depth distribution of known vent fields among MORs (red bars), BASCs (blue bars), and arcs (green bars). The peak at 2300–2800 m corresponds to the predominant axial depth of OSRs. Figure adapted from Beaulieu et al. (2013).

Fig. 9. Jurisdictional distribution of vent fields before 2000 (red bars) and presently (blue bars) among the High Seas and countries with >10 known vent fields in their Exclusive Economic Zones. Vent exploration in the western Pacific since 2000 has greatly increased the known vent population in the EEZs of several countries. Figure adapted from Beaulieu et al. (2013).

Fig. 10. Examples of hydrothermal vent exploration conducted primarily by systematic vertical casts. (a) A 2004 survey of the Fonualei Rift and Spreading Center, a BASC just west of the Kermadec arc. Vertical black lines show locations of individual profiles from which the contoured LBS data were derived. Note that the contouring is coarse, creating arbitrary plume dimensions and long ridge areas of no information. Figure adapted from German et al. (2006). (b) Expeditions in 1999 and 2002 along the Kermadec arc. Hash marks at the panel top mark vertical casts by a CTD/sensor package, occasionally supplemented by CTD/sensor tows (e.g., at volcanoes near 31° and 35°S). LBS anomalies above various volcano summits mark active hydrothermal activity. The white vertical line separates the two surveys. Data from the two surveys were gridded and contoured separately; differences in the surface layer are due to the time separating the two surveys and seasonal influences. Figure adapted from de Ronde et al. (2007).

Fig. 11. Example of hydrothermal vent exploration conducted primarily by tows along the superfast-spreading southern East Pacific Rise (Baker et al., 2002; Walker et al., 2004). (a) Combined LBS plume anomalies from six CTD/sensor tow-yos. (b) Detail of portions of two overlapping tow-yos showing the CTD/sensor path between ~2000 and 2400 m (black sawtooth pattern). (c) Detail of the same plumes mapped ~1 day later using a horizontally towed side-scan sonar vehicle with six LBS sensors attached to the tow line (black quasi-horizontal lines). A high-temperature vent field was discovered in 1999 at 31.15°, where the LBS anomalies are closest to the seafloor (Lupton et al., 1999), but many other vent fields are also likely.

Fig. 12. Indicators of hydrothermal activity along the northern East Pacific Rise. Data collected by single ORP and LBS sensors on a remotely operated vehicle ~60 m above bottom. (a) Distribution of InterRidge sites (black arrows) and sites determined by this survey (yellow circles). Multiple sites occur in a small area near 9.65°–9.68°N. (b) Continuous ORP (red) and

LBS (blue, given in Nephelometric Turbidity Units) data. (c) Locations of active vents (enumerated vents, red bars) and diffuse flow or vent biology (presence/absence only, cyan bars) from historical camera tows and submersible observations, binned at 0.93 km (0.0083°) intervals (Haymon et al., 1991; Haymon and White, 2004). Following Haymon and White (2004), areas south of 9.45ºN with low (1–4) animal frequencies are not included here. Figure adapted from Baker et al. (2016).

Fig. 13. Indicators of hydrothermal activity along the eastern Galápagos Spreading Center. Data collected west of 89.6°W by an ORP sensor on a tow package ~120 m above bottom and by LBS sensors arrayed along the towline (as in Fig. 11c), and east of 89°W by ORP and LBS sensors on a towed instrument package continuously cycled between 300 m and 20 m above bottom (as in Fig. 11b). (a) Distribution of InterRidge sites (black arrows) and sites detected by this survey (yellow circles). (b) Continuous ORP (red) and LBS (blue) data. Figure adapted from Baker et al. (2016).

Fig. 14. Indicators of hydrothermal activity along the Eastern Lau Spreading Center. Data collected along two parallel track lines, nominally ~600 m apart, by an ORP sensor on a tow package ~120 m above bottom and by LBS sensors arrayed along the towline. (a) Distribution of InterRidge sites (black arrows) and sites determined by this survey (yellow circles). (b) Continuous ORP (red and orange) and LBS (blues) data for both track lines. Figure adapted from Baker et al. (2016).

Fig. 15. (a) Brothers Caldera, with Autonomous Underwater Vehicle (AUV)-derived bathymetry overlain on surface-ship bathymetry using EM300 sonar. Tracks of eight 2007 AUV dives and one 2011 AUV dive shown by colored lines. (b) Distribution of ORP anomalies, here displayed as the time derivative (dORP/dt (mV/s) anomalies, color-coded to plume intensity, which increases as dORP/dt values become more negative). (c) Summary of predicted hydrothermal discharge types in Brothers Caldera and cones, based on the areal distributions of anomalies of turbidity, ORP, and temperature. Figure adapted from Baker et al. (2012).

Fig. 16. Scatter plot of site frequency (left axis) and site separation (right axis) vs. spreading rate for 27 ridge sections using data from the InterRidge Database (red dots) (see Fig. 5). The three sections shown in Figs. 12–14, plus additional data from other ridge sections, are symbol-coded: eastern Galápagos Spreading Center (eGSC, inverted triangles), central Galápagos Spreading Center (cGSC, circles), Eastern Lau Spreading Center (ELSC, diamonds), northern East Pacific Rise (nEPR, squares), and southern East Pacific Rise (sEPR, skewed triangles). Results for these sections are from InterRidge Database (large red symbols), Baker et al. (2016) (green), and results from visual seafloor observations (Haymon et al., 1991; Haymon and White, 2004) (purple). InterRidge values for the nEPR and sEPR (large red symbols) are for portions of the full sections (red dots) where ORP data and/or seafloor observations are available. Double-headed horizontal arrow for the ELSC indicates the range of spreading rates for that ridge section. All other sections have uniform spreading rates. Figure adapted from Baker et al. (2016).

Table 1. Standard survey results from ridge sections longer than 200 km (Beaulieu et al., 2015).

Region	Surveyed portion	Length (km)	Mean full spreading rate (mm/yr)	Known vent fields	Vent field frequency (sites/100 km)	Mean vent spacing (km)
SWIR	58.5°-60.5°E & 63.5°-66°E	430	9.8	7	1.6	61
Gakkel Ridge	6°W-85°E	965	11.8	9	0.9	108
SWIR	49°-52°E	270	11.9	4	1.5	68
SWIR	10°-16°E	416	13.5	6	1.4	69
SWIR	16°-23°E	484	13.7	2	0.4	244
Reykjanes Ridge	57.7°-63°N	750	19.8	3	0.4	250
N MAR	35.7°-38°N	340	20.3	12	3.5	28
N MAR	27°-30°N	375	23.1	3	0.8	125
N MAR	11°-21°N	935	25.5	15	1.6	62
Woodlark Ridge	151.5°-155.8°E	520	30.6	3	0.6	172
Carlsberg Ridge	2°-4.5°N	440	30.7	2	0.5	222
S MAR	2.5°-6.8°S	450	32.4	2	0.4	227
S MAR	7°-11°S	450	33.2	4	0.9	113
CIR	8°-17°S	738	36.2	10	1.4	74
CIR	18.3°-20.8°S	300	42.3	3	1	100
Galápagos Ridge	89.5°-95.5°W	560	53.2	8	1.4	70
Gorda Ridge	41°-43°N	240	55.6	5	2.1	48
JdFR	44.5°-48.3° N	480	56.1	19	4.0	25
ELSC/VFR	19.5°-23°S	400	64.4	32	8	12
SEIR	36-40°S	445	64.4	2	0.5	222
SEIR	77-100°E	1600	68.1	37	1.8	56
N EPR	15.5-18.5°N	335	77	6	1.8	56
NELSC, MTJ, FRSC	14.7°-17.7°S	340	87.6	14	4.1	24
N EPR	8.7-13.2°N	515	98.1	21	4.1	24
Manus Basin	148°-152°E	405	101.4	11	2.7	37
S EPR	13.5-18.6°S	585	145.4	24	4.1	24
S EPR	27.5-32.3°S	440	158.3	14	3.2	31

Abbreviations: SWIR, Southwest Indian Ridge; MAR, Mid-Atlantic Ridge; CIR, Central Ridge; JdFR, Juan de Fuca Ridge; ELSC, Eastern Lau Spreading Center; VFR, Valu Fa Ridge; SEIR, Southeast Indian Ridge; NELSC, Northeast Lau Spreading Center; MTJ; MangatoluTriple Junction; FRSC, Fonualei Ridge Spreading Center; EPR, East Pacific Rise. Further details about each section can be found in Beaulieu et al. (2015).

Table 2. Best practices survey results from ridge sections longer than 200 km.

Region	Surveyed portion	Length (km)	Mean full spreading rate (mm/yr)	Known vent fields	Vent field frequency (sites/100 km)	Mean vent spacing (km)
Galápagos Ridge	91°-94.9°W	430	53.2	33	7.7	13
Galápagos Ridge	85.8°-90.6°W	520	60	29	5.6	19
ELSC/VFR	19.3°-22.8°S	420	64.4	96	22.8	4.2
N EPR	9°-10°N	110	100	27	24.5	4.1

Abbreviations: ELSC, Eastern Lau Spreading Center; VFR, Valu Fa Ridge; EPR, East Pacific Rise.

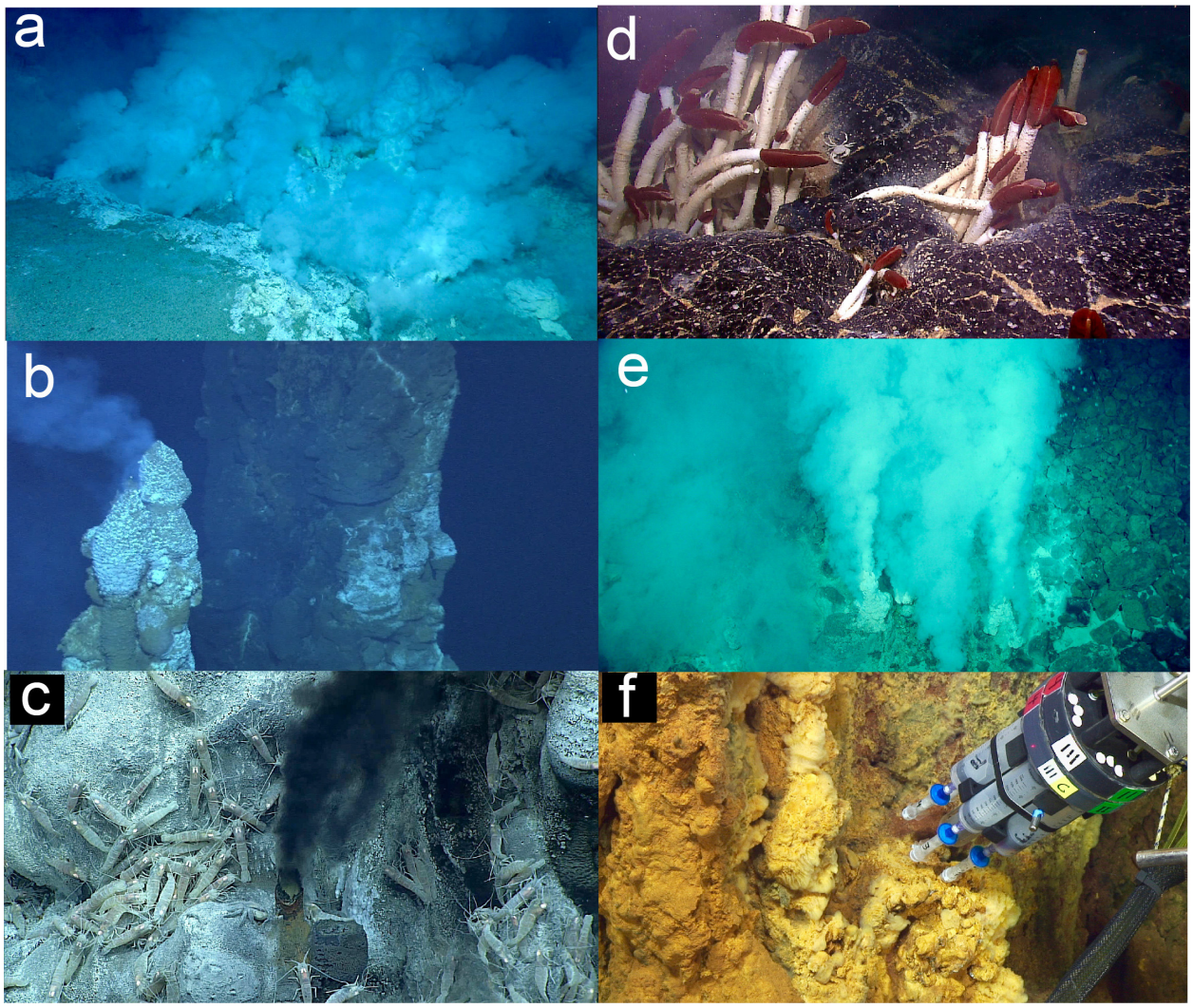
a
d
b
e
c
f

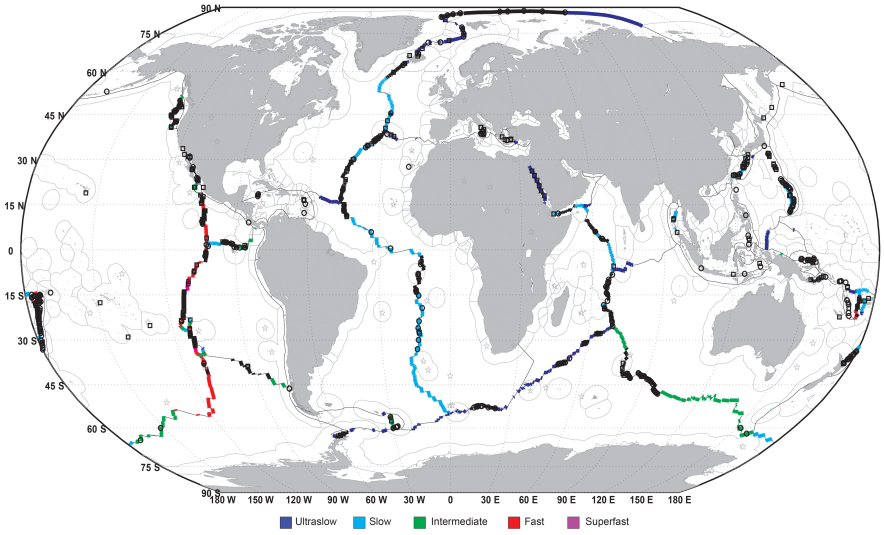
90 N
75 N
60 N
45 N
30 N
15 N
0
15 S
30 S
45 S
60 S
75 S
90 S
180 W
150 W
120 W
90 W
60 W
30 W
0
30 E
60 E
90 E
120 E
150 E
180 E
Ultraslow
Slow
Intermediate
Fast
Superfast

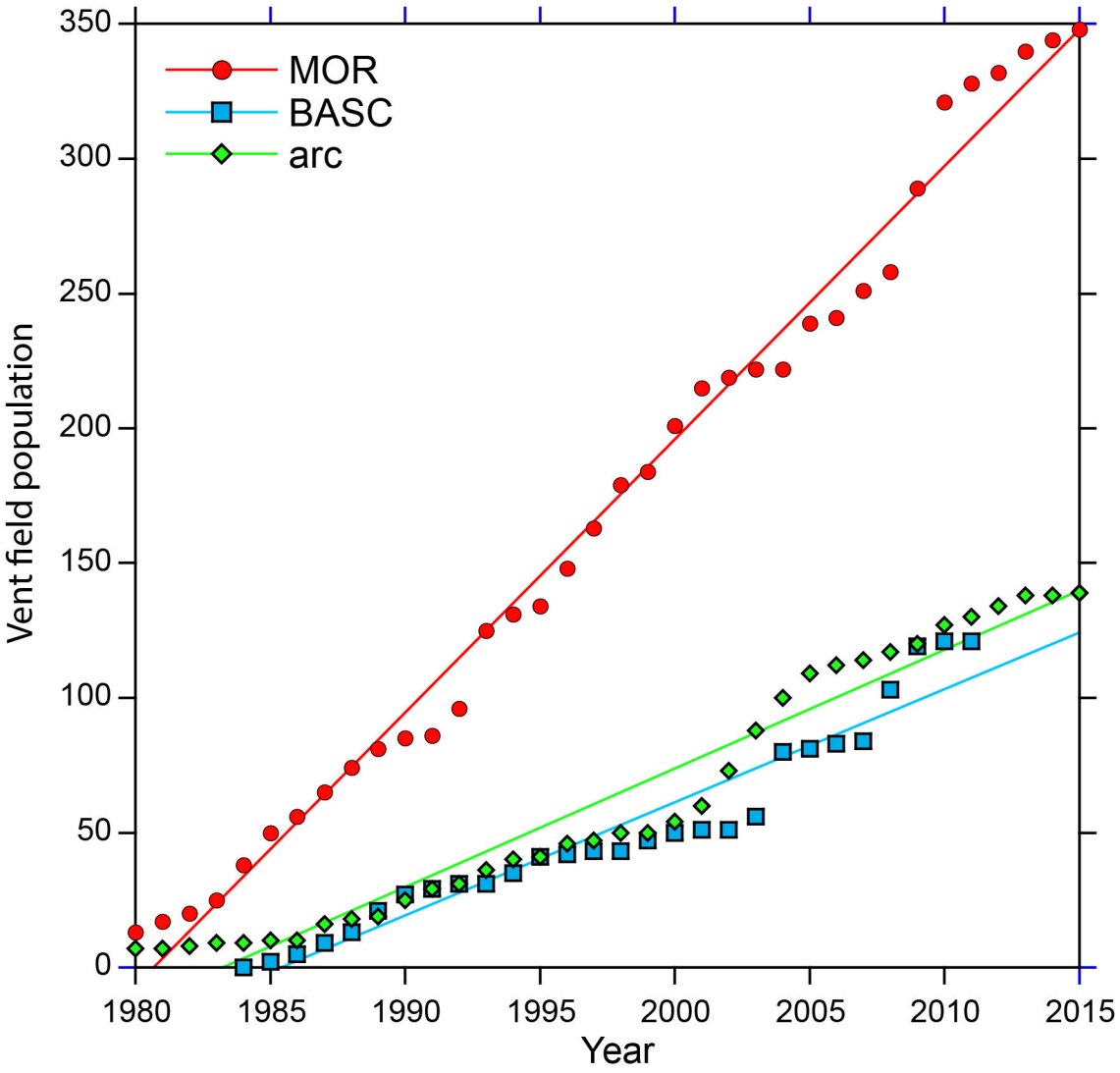
MOR
BASC
arc
Vent field population
Year
0
50
100
150
200
250
300
350
1980
1985
1990
1995
2000
2005
2010
2015

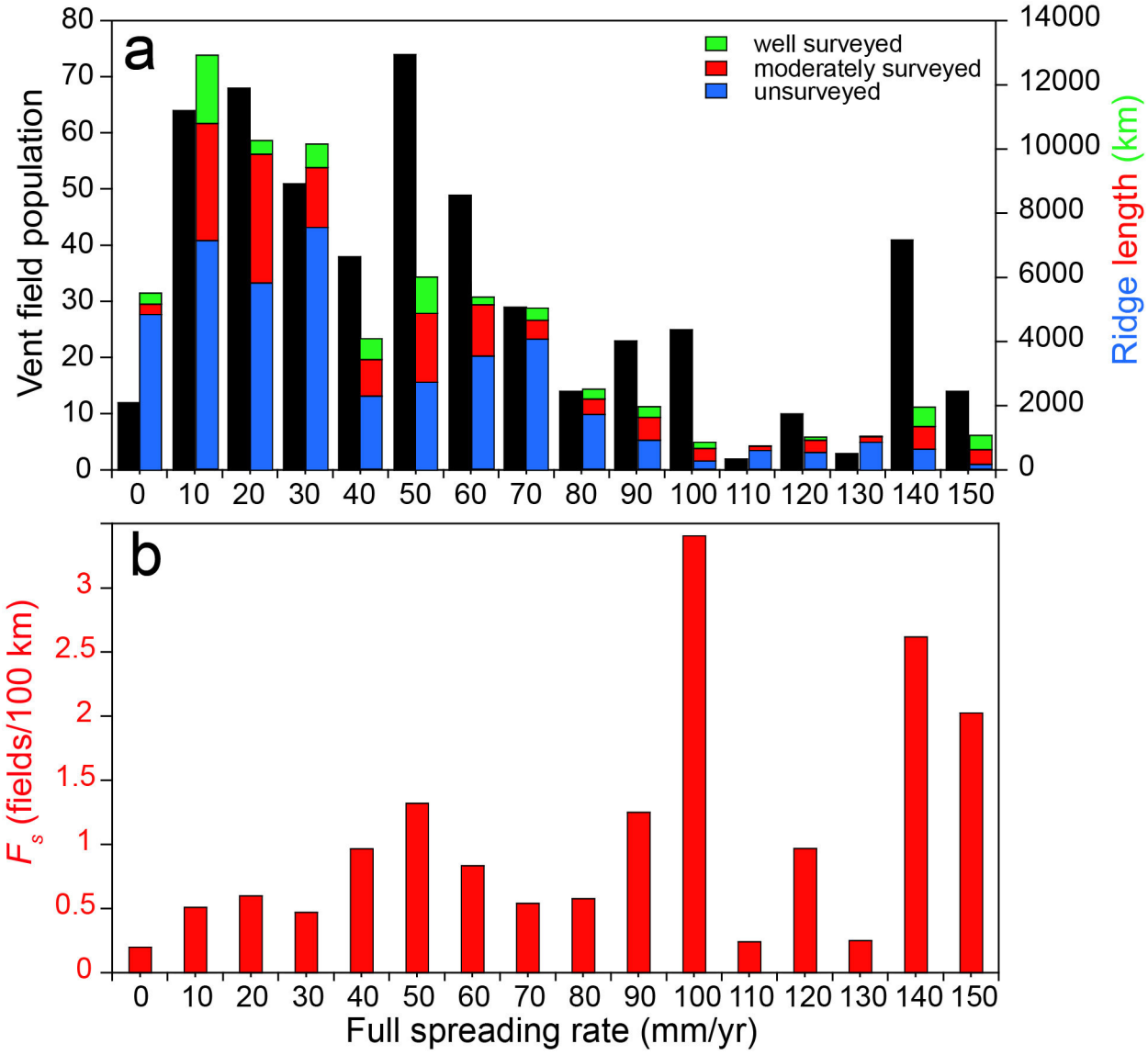
a
well surveyed
moderately surveyed
unsurveyed
Vent field population
Ridge length (km)
0
10
20
30
40
50
60
70
80
90
100
110
120
130
140
150
0
2000
4000
6000
8000
10000
12000
14000
b
F_s (fields/100 km)
0
0.5
1
1.5
2
2.5
3
Full spreading rate (mm/yr)

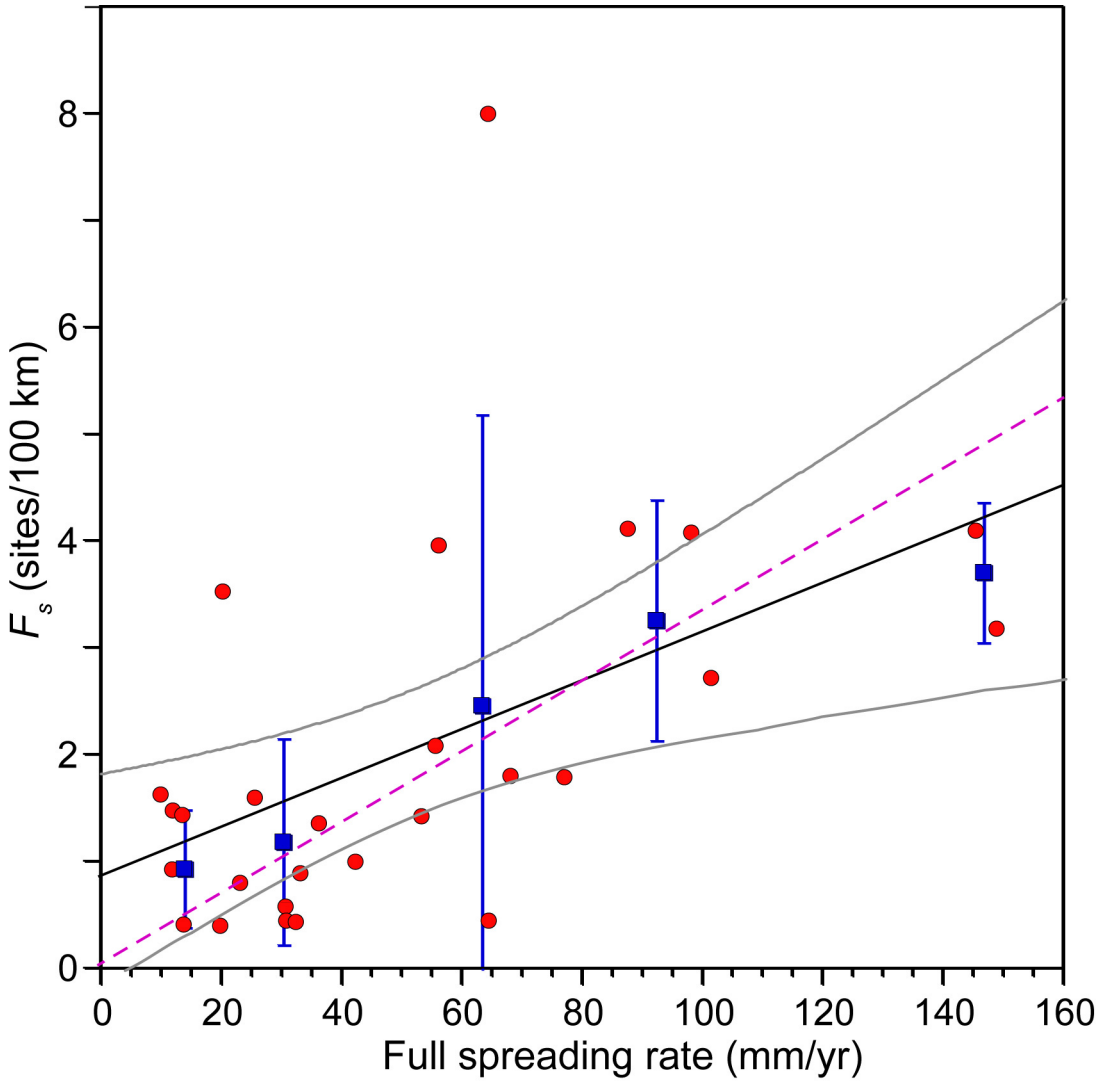
8
6
4
2
0
F_s (sites/100 km)
0
20
40
60
80
100
120
140
160
Full spreading rate (mm/yr)

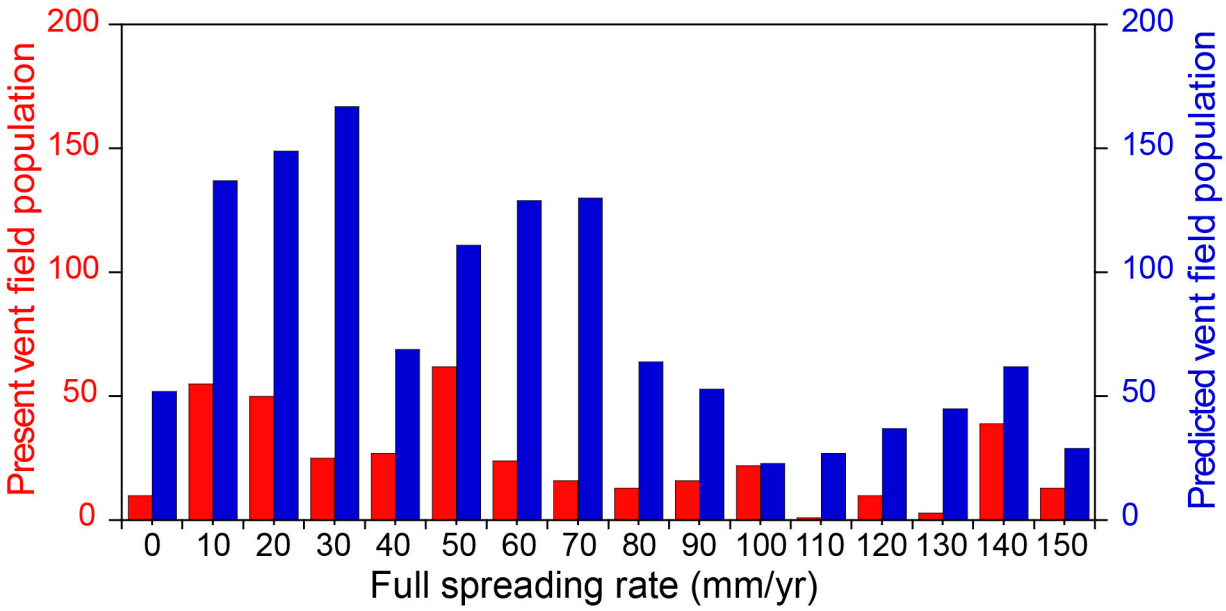
Present vent field population
Predicted vent field population
Full spreading rate (mm/yr)
0
50
100
150
200
0
10
20
30
40
50
60
70
80
90
100
110
120
130
140
150

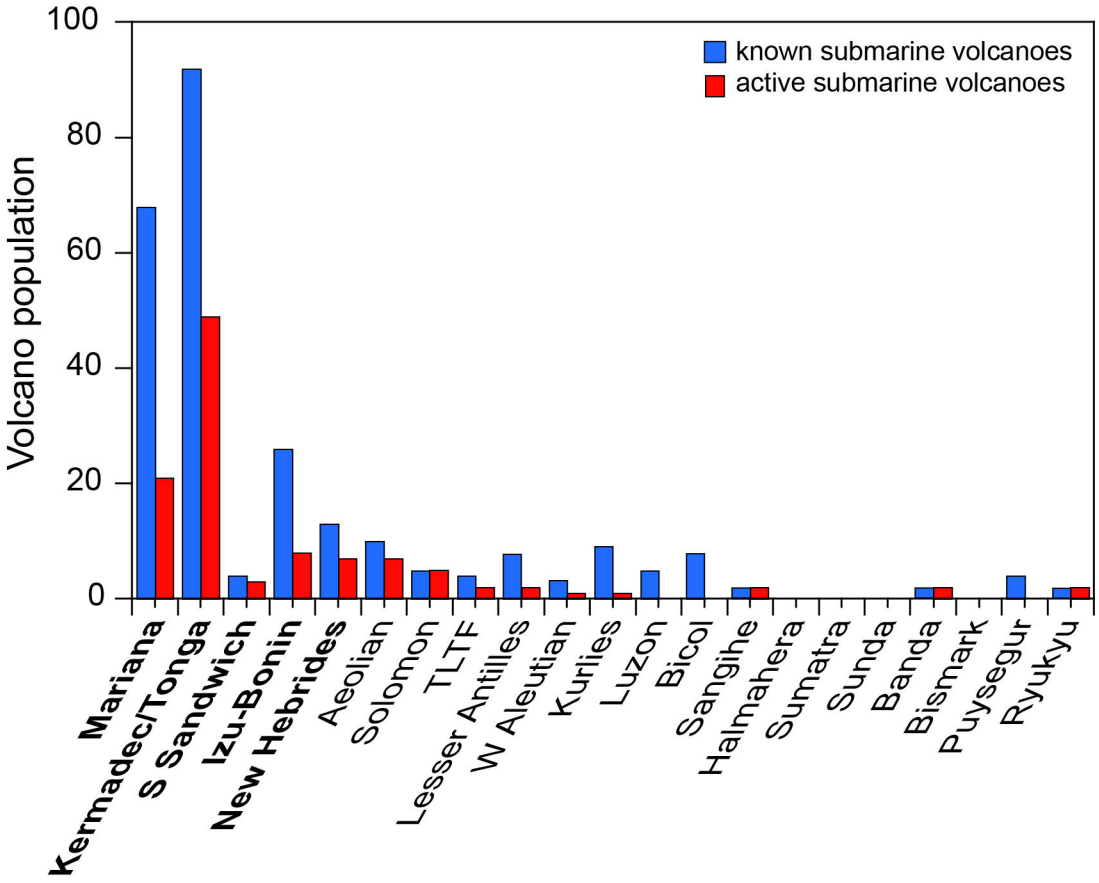
100
80
60
40
20
0
Volcano population
known submarine volcanoes
active submarine volcanoes
Mariana
Kermadec/Tonga
S Sandwich
Izu-Bonin
New Hebrides
Aeolian
Solomon
TLTF
Lesser Antilles
W Aleutian
Kurlies
Luzon
Bicol
Sangihe
Halmahera
Sumatra
Sunda
Banda
Bismark
Puysegur
Ryukyu

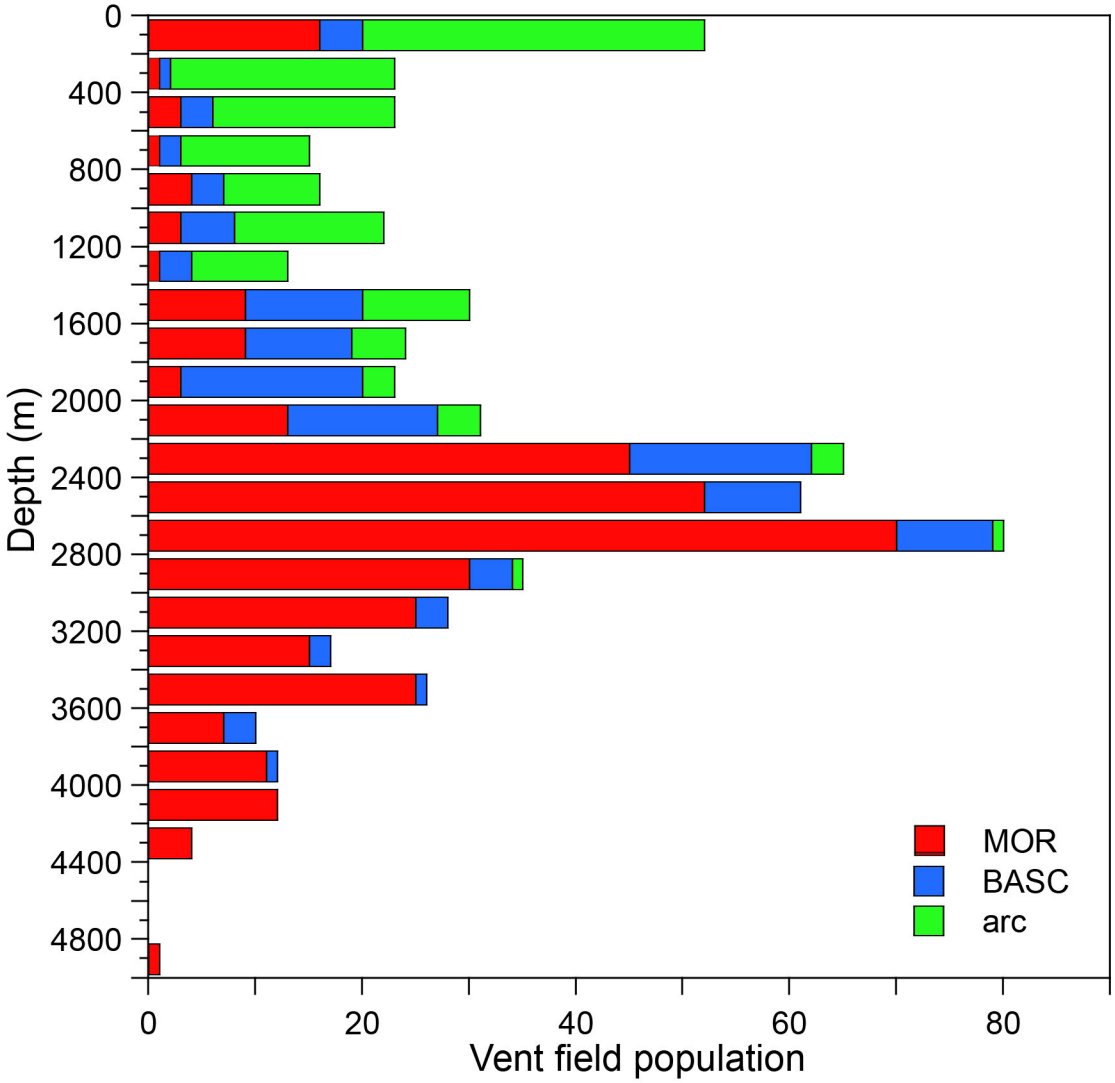
Depth (m)
0
400
800
1200
1600
2000
2400
2800
3200
3600
4000
4400
4800
0
20
40
60
80
Vent field population
MOR
BASC
arc

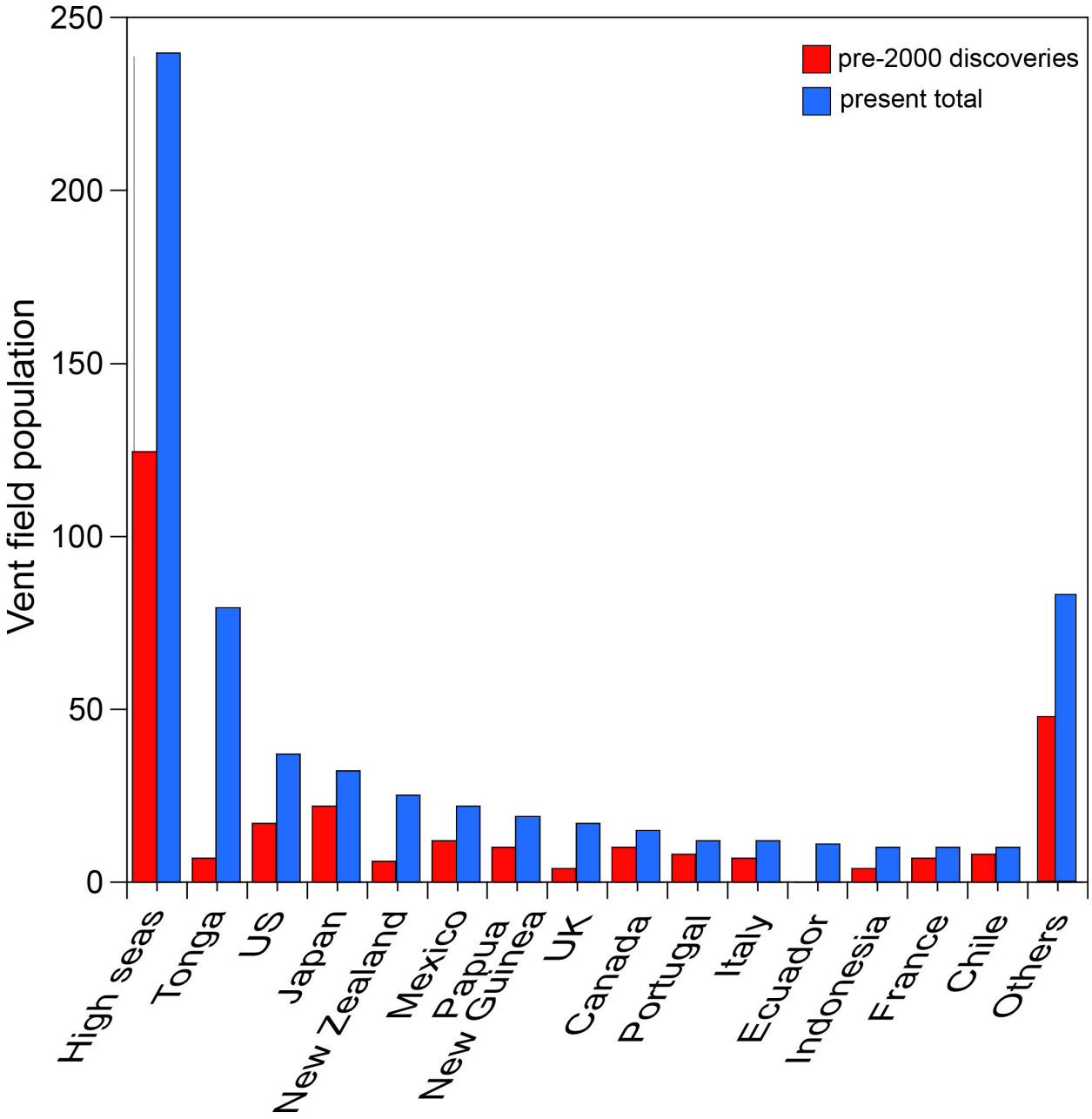
250
200
150
100
50
0
Vent field population
pre-2000 discoveries
present total
High seas
Tonga
US
Japan
New Zealand
Mexico
Papua New Guinea
UK
Canada
Portugal
Italy
Ecuador
Indonesia
France
Chile
Others

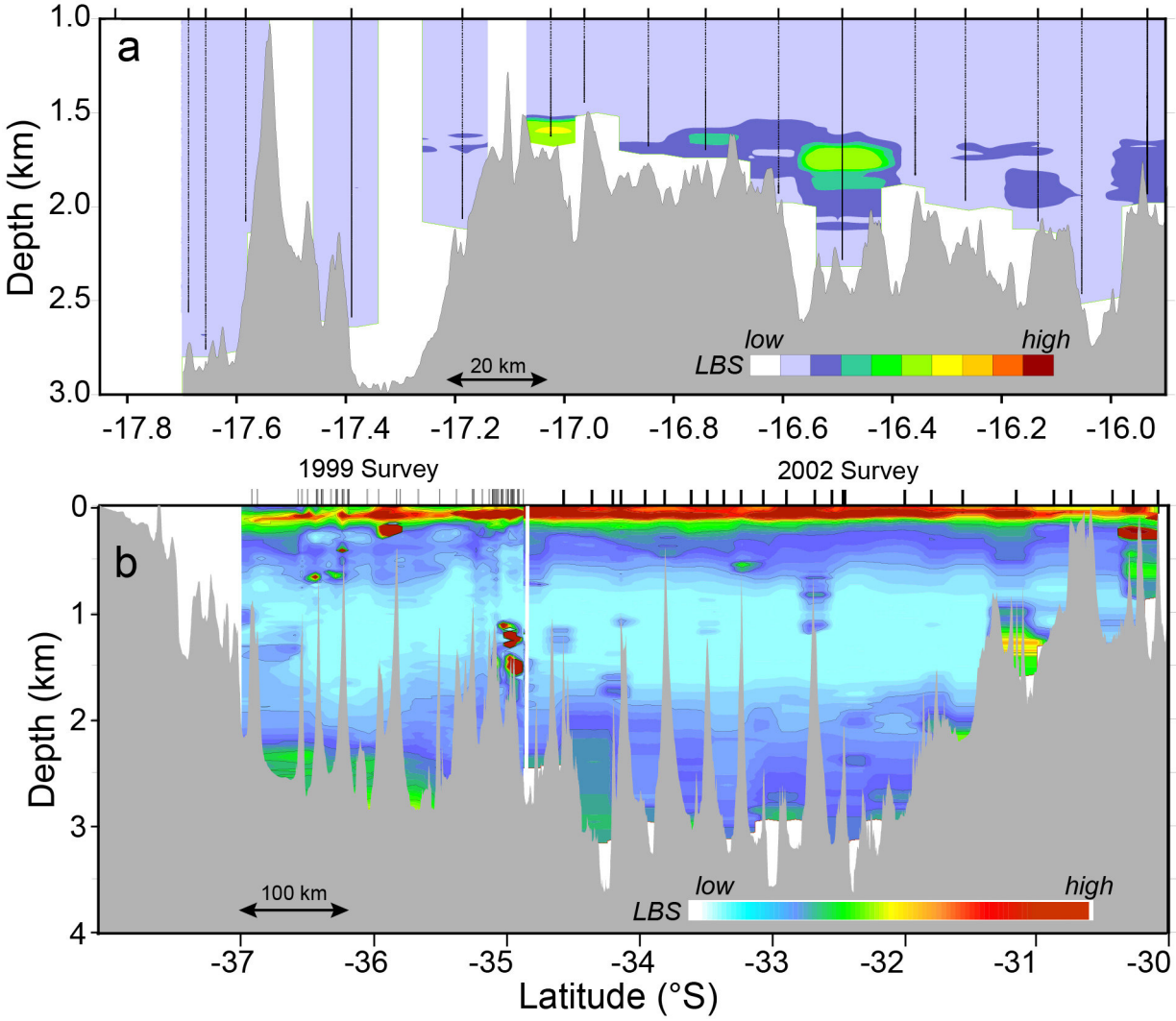
a
Depth (km)
1.0
1.5
2.0
2.5
3.0
20 km
low
high
LBS
-17.8
-17.6
-17.4
-17.2
-17.0
-16.8
-16.6
-16.4
-16.2
-16.0
1999 Survey
2002 Survey
b
Depth (km)
0
1
2
3
4
100 km
low
high
LBS
-37
-36
-35
-34
-33
-32
-31
-30
Latitude (°S)

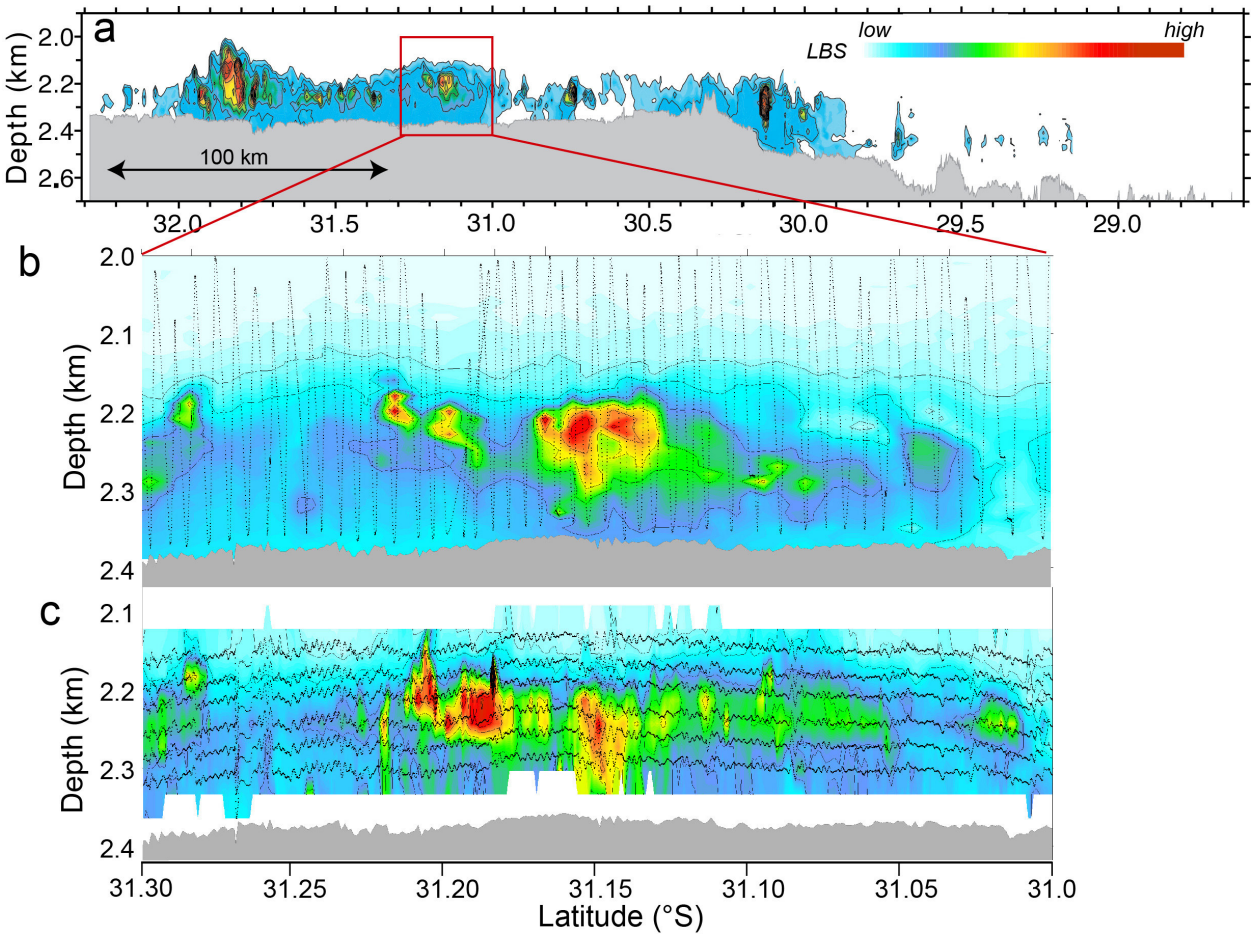
a
low
high
LBS
Depth (km)
2.0
2.2
2.4
2.6
100 km
32.0
31.5
31.0
30.5
30.0
29.5
29.0
b
Depth (km)
2.0
2.1
2.2
2.3
2.4
c
Depth (km)
2.1
2.2
2.3
2.4
31.30
31.25
31.20
31.15
31.10
31.05
31.0
Latitude (°S)

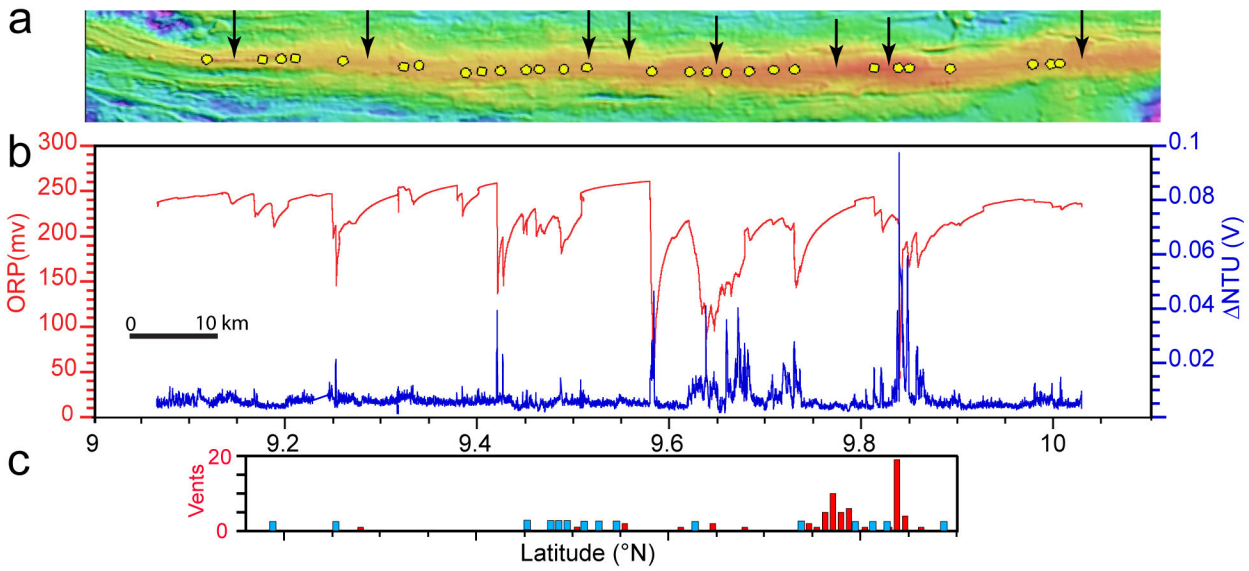
a
b
c
ORP(mv)
ΔNTU (V)
0
10 km
Vents
Latitude (°N)

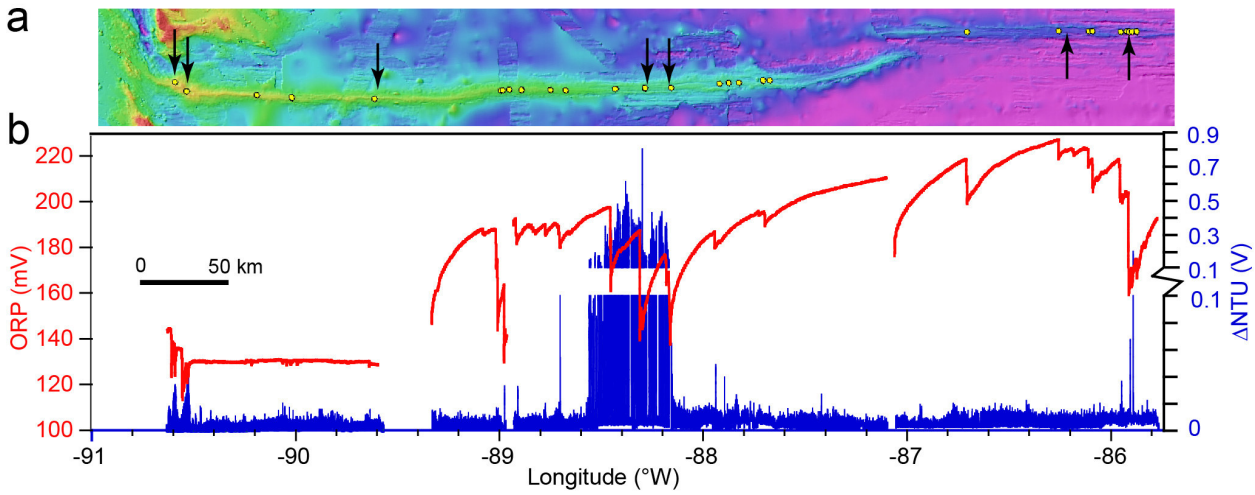
a
b
220
200
180
160
140
120
100
ORP (mV)
0
50 km
0.9
0.7
0.5
0.3
0.1
0.1
0
ΔNTU (V)
-91
-90
-89
-88
-87
-86
Longitude (°W)

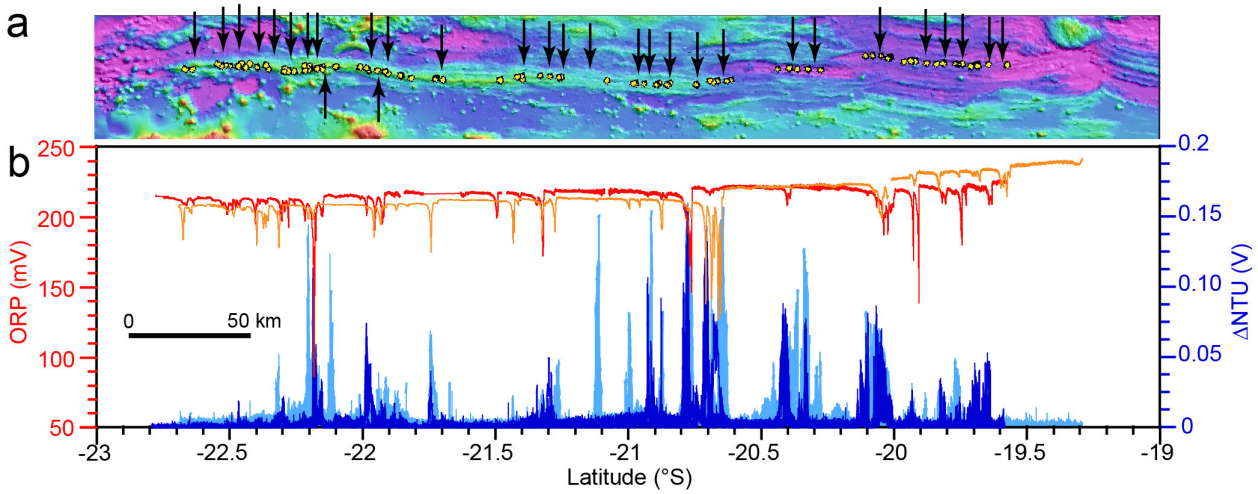
a
b
250
200
150
100
50
ORP (mV)
0
50 km
0.2
0.15
0.10
0.05
0
ΔNTU (V)
-23
-22.5
-22
-21.5
-21
-20.5
-20
-19.5
-19
Latitude (°S)

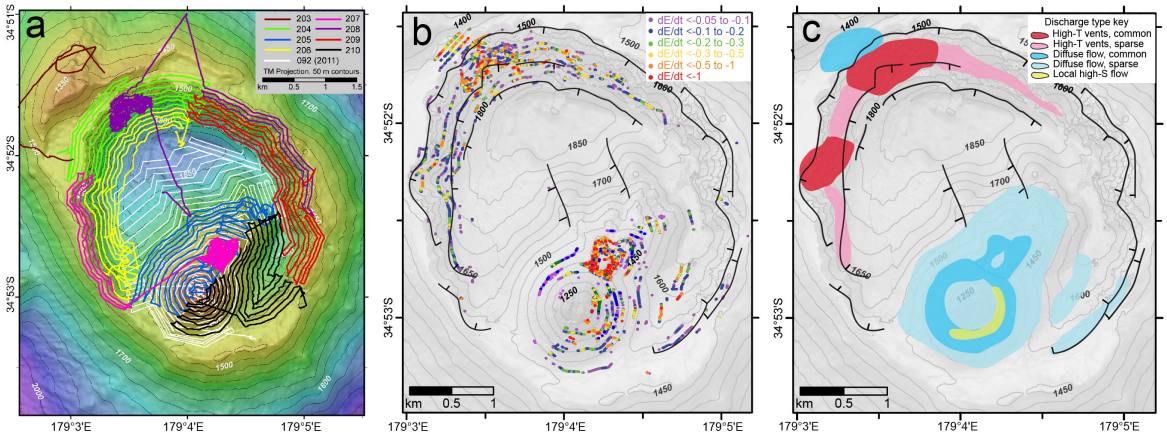
a
203
204
205
206
092 (2011)
207
208
209
210
TM Projection. 50 m contours
km 0.5 1 1.5
b
dE/dt <-0.05 to -0.1
dE/dt <-0.1 to -0.2
dE/dt <-0.2 to -0.3
dE/dt <-0.3 to -0.5
dE/dt <-0.5 to -1
dE/dt <-1
c
Discharge type key
High-T vents, common
High-T vents, sparse
Diffuse flow, common
Diffuse flow, sparse
Local high-S flow
34°51'S
34°52'S
34°53'S
179°3'E
179°4'E
179°5'E
km 0.5 1

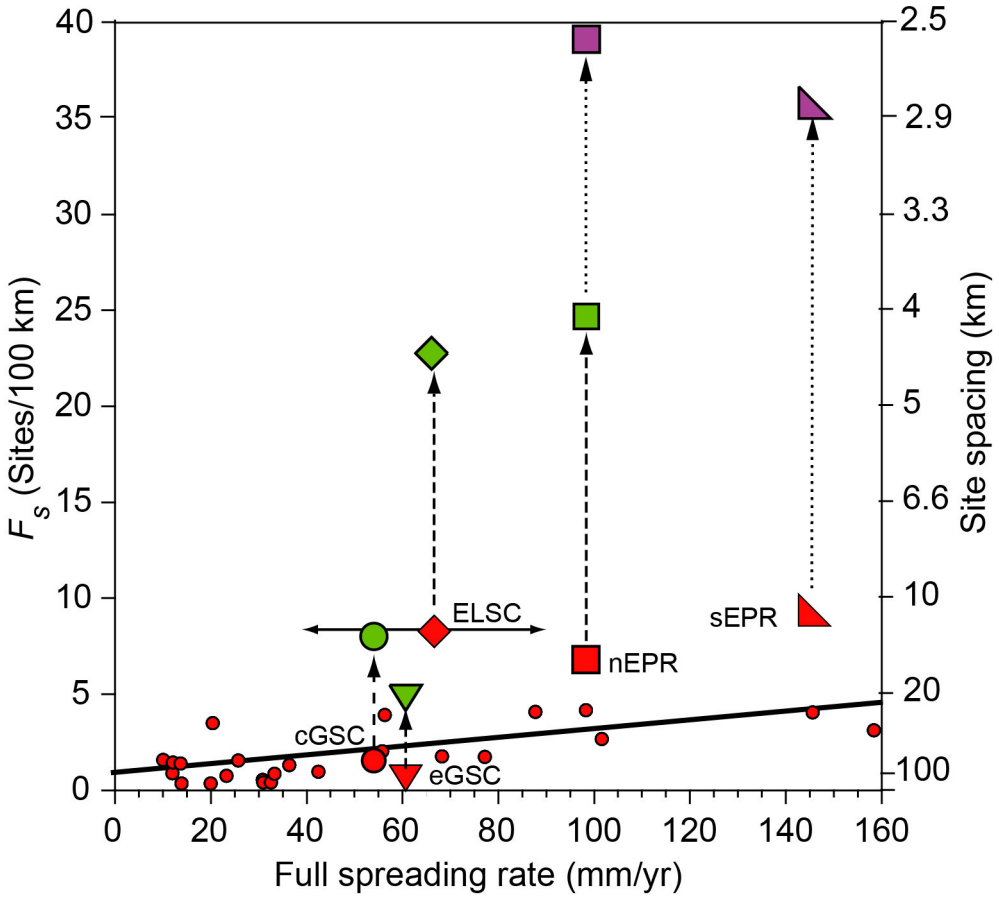
40
35
30
25
20
15
10
5
0
F_s (Sites/100 km)
2.5
2.9
3.3
4
5
6.6
10
20
100
Site spacing (km)
0
20
40
60
80
100
120
140
160
Full spreading rate (mm/yr)
ELSC
nEPR
sEPR
cGSC
eGSC

- Four decades of ocean exploration have discovered >630 submarine hydrothermal sites
- 80% of sites occur on ocean ridges; site frequency increases with spreading rate
- New exploration methods suggest a 3-6× underestimation of site frequency on ridges
- Underestimation hinders quantitative modeling of important Earth-ocean interactions

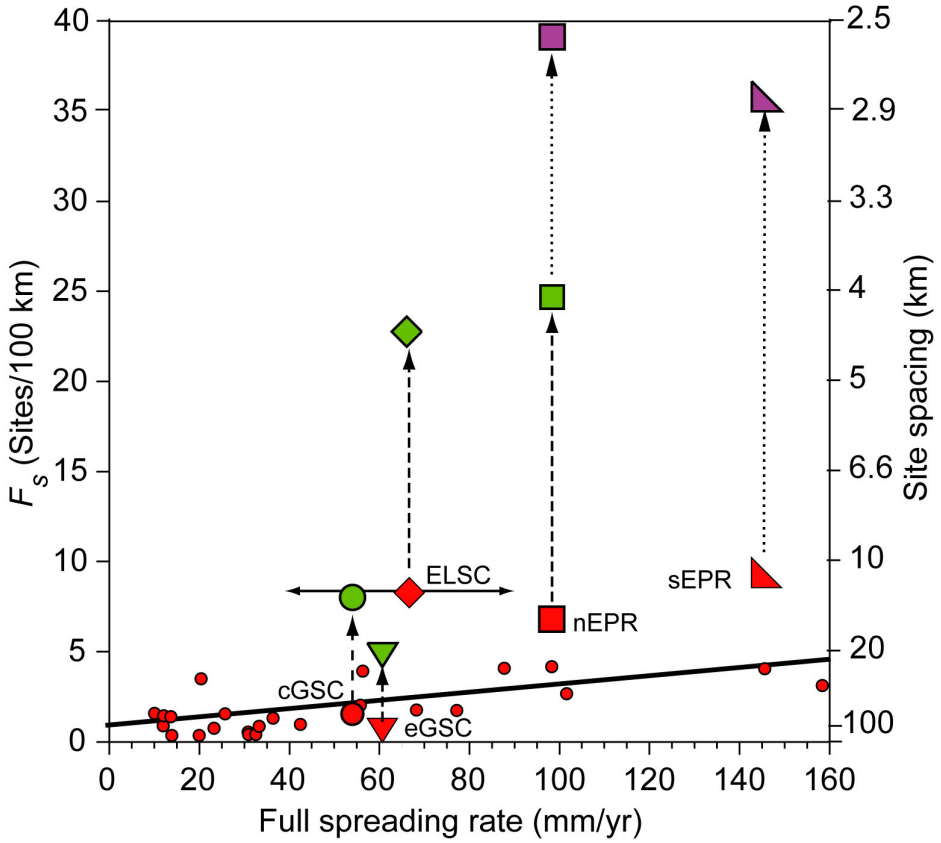
40
35
30
25
20
15
10
5
0
F_s (Sites/100 km)
2.5
2.9
3.3
4
5
6.6
10
20
100
Site spacing (km)
0
20
40
60
80
100
120
140
160
Full spreading rate (mm/yr)
ELSC
nEPR
sEPR
cGSC
eGSC